UNIVERSIDADE FEDERAL DO CEARÁ
CENTRO DE TECNOLOGIA
DEPARTAMENTO DE ENGENHARIA METALÚRGICA E DE MATERIAIS
PROGRAMA DE PÓS-GRADUAÇÃO EM ENGENHARIA E CIÊNCIA DE MATERIAIS

JOSÉ RENÊ DE SOUSA ROCHA

MODELING AND NUMERICAL SIMULATION OF FLUID FLOW AND HEAT TRANSFER OF A STEEL CONTINUOUS CASTING TUNDISH

FORTALEZA
2017

JOSÉ RENÊ DE SOUSA ROCHA

MODELING AND NUMERICAL SIMULATION OF FLUID FLOW AND HEAT TRANSFER OF A STEEL CONTINUOUS CASTING TUNDISH

Dissertação submetida ao Programa de Pós-Graduação em Engenharia e Ciência de Materiais da Universidade Federal do Ceará como requisito parcial à obtenção do título de Mestre em Engenharia e Ciência de Materiais. Área de Concentração: Processos de transformação e degradação dos materiais.

Orientador: Prof. Dr. Francisco Marcondes

FORTALEZA

2017

Dados Internacionais de Catalogação na Publicação
Universidade Federal do Ceará
Biblioteca Universitária
Gerada automaticamente pelo módulo Catalog, mediante os dados fornecidos pelo(a) autor(a)

R573m Rocha, José Renê de Sousa.
Modeling and numerical simulation of fluid flow and heat transfer of a steel continuous casting tundish / José Renê de Sousa Rocha. – 2017.
91 f. : il. color.

Dissertação (mestrado) – Universidade Federal do Ceará, Centro de Tecnologia, Programa de Pós-Graduação em Engenharia e Ciência de Materiais, Fortaleza, 2017.
Orientação: Prof. Dr. Francisco Marcondes.

1. Numerical simulation. 2. Steel continuous casting tundish. 3. Finite-volume method. I. Título.
CDD 620.11

JOSÉ RENÊ DE SOUSA ROCHA

MODELING AND NUMERICAL SIMULATION OF FLUID FLOW AND HEAT TRANSFER OF A STEEL CONTINUOUS CASTING TUNDISH

Dissertação submetida ao Programa de Pós-Graduação em Engenharia e Ciência de Materiais da Universidade Federal do Ceará como requisito parcial à obtenção do título de Mestre em Engenharia e Ciência de Materiais. Área de Concentração: Processos de transformação e degradação dos materiais.

Aprovada em: 17/02/2017.

BANCA EXAMINADORA

_____

Prof. Dr. Francisco Marcondes (Supervisor)
Federal University of Ceará (UFC)

_____

Prof. Dr. Clovis Raimundo Maliska
Federal University of Santa Catarina (UFSC)

_____

Prof. Dr. Janaína Gonçalves Maria da Silva Machado
Federal University of Ceará (UFC)

_____

Dr. Eng. Alex Maia do Nascimento
Gerdau Company

To God.
To my parents, Pedro and Celina.

ACKNOWLEDGEMENTS

First of all, I would like to thank my family, specially my parents, Pedro and Celina, for all support during these years that I have been at Federal University of Ceará, for their good advices and guidance to succeed in all steps of my life.

I am thankful to all professors who I had the opportunity to study during these two years at the Graduate Program in Engineering and Material Science, besides, I would also like to express my gratitude for their help and effort to transmit some fundamental knowledge to us. Amongst the professors, I would like to thank my supervisor, Francisco Marcondes, with whom I had the opportunity to develop this study. In addition, I thank him for his fundamental experience during the supervision of this research, his helpful tips and review of this text, and all his collaboration during the development of this thesis.

I am also grateful to the committee members, composed by prof. Dr. Francisco Marcondes, prof. Dr. Clovis Raimundo Maliska, prof. Dr. Janaína Gonçalves Maria da Silva Machado, and Dr. Eng. Alex Maia do Nascimento, for their availability in being part of this work.

I would like to thank my classmates and friends for the great moments of joy and studies throughout this long journey of hard work. Furthermore, I would like to recognize the great advices, comments, and the significant sharing of information that I have received from my friends from the Computational Fluid Dynamics Laboratory (LDFC) and especially thank to Ivens, whose guidance at earlier stages of this thesis brought some fundamental contribution to this work to be finished.

Last but not least, I would like to acknowledge the financial support provided by CNPq (The National Council of Technological and Scientific Development) to this research and the Gerdau Company for making available to us the actual tundish parameters.

“We should all be concerned about the future because we will have to spend the rest of our lives there.”

“Charles F. Kettering”

ABSTRACT

Currently, the continuous casting process is the most used technique to produce steel. Being an inherently component of the caster machine, the tundish has been designed to be not only an intermediate vessel between the ladle and the mold, but also a device to remove inclusions and a metallurgical reactor. Therefore, the tundish has an important role in the continuous casting process. The physical model for heat transfer and fluid flow into the tundish is very complex, thus analytical solutions are not available. Physical studies might present many difficulties for analyzing the process. Hence, Computational Fluid Dynamics (CFD) emerges as an attractive alternative. CFD is based on numerical approaches that are used to solve several classes of engineering problems. The main goal of the present study is to analyze the fluid flow and temperature fields into an actual tundish configuration that is used in continuous casting processes of a local steelmaker company. Based on the performed simulations, some modifications in the geometry of the tundish are proposed in order to improve the steel quality; these modifications make use of weirs and dams. For solving the governing equations arising from the physical model, the Ansys CFX software, which is based on the Element-based Finite-Volume Method (EbFVM) were used. Simulations were performed using water and steel as working fluids for a turbulent flow in a 3D tundish. The results were presented in terms of velocity and temperature fields and Residence Time Distribution (RTD) curves, which evaluated them qualitatively and quantitatively.

Keywords: Numerical Simulation, Steel Continuous Casting Tundish, RTD, Ansys CFX, EbFVM, Finite-Volume Method.

RESUMO

O processo de lingotamento contínuo é o processo mais utilizado na produção de aço atualmente. Sendo um importante componente da máquina de lingotamento, o distribuidor tem sido projetado para atuar não apenas como um reservatório entre a panela e o molde, mas também como um dispositivo para remoção de inclusões e servir como um reator metalúrgico. Logo, o distribuidor assume um papel de relevância no processo de lingotamento contínuo. O modelo físico que rege a transferência de calor e escoamento dentro do distribuidor apresenta grande complexidade, tornando a sua solução analítica indisponível. Estudos físicos podem apresentar várias dificuldades para a análise do processo. Portanto, a Dinâmica dos Fluidos Computacional (CFD) surge com uma alternativa viável. CFD é baseada em aproximações numéricas as quais são utilizadas para a solução de várias classes de problemas de engenharia. O principal objetivo do presente trabalho é analisar os campos de escoamento e temperatura no interior de um distribuidor o qual é utilizado nos processos de lingotamento contínuo de uma companhia siderúrgica local. Com base nas simulações realizadas, modificações na geometria do distribuidor são propostas com o intuito de aumentar a qualidade do aço. Essas modificações são feitas através do uso de diques e barragens. Para a solução das equações de conservação originadas do modelo físico, o programa Ansys CFX, o qual utiliza o Método dos Volumes Finitos baseado em Elementos (EbFVM), foi utilizado. As simulações foram feitas utilizando-se aço e água como fluidos de trabalho para um escoamento turbulento em um distribuidor tridimensional. Os resultados foram apresentados em termos de campos de velocidade e temperatura e curvas de Distribuição de Tempo de Residência (RTD) as quais serviram para analisá-los qualitativa e quantitativamente.

Palavras-chave: Simulação Numérica, Distribuidor de Lingotamento Contínuo de Aço, RTD, Ansys CFX, EbFVM, Método de Volumes Finitos.

LIST OF FIGURES

LIST OF TABLES

LIST OF ABBREVIATIONS

AISI	American Iron and Steel Institute
CFD	Computational Fluid Dynamics.
CNPq	National Council of Technological and Scientific Development (Conselho Nacional de Desenvolvimento Científico e Tecnológico)
DNS	Direct Numerical Simulation
EbFVM	Element-based Finite-Volume Method
FDM	Finite Difference Method
FEM	Finite Element Method
FVM	Finite Volume Method
LDA	Laser Doppler Anemometer
LES	Large Eddy Simulation.
RANS	Reynolds Averaged Navier-Stokes
RMS	Root Mean Square
RNG	Re-Normalized Group
RSM	Reynolds Stress Model
RTD	Residence Time Distribution
RWM	Random Walk Model

LIST OF SYMBOLS

a_1 Constant for SST turbulence model.

C Dimensionless concentration.

C_D Drag coefficient.

C_p Specific heat at constant pressure, [$J/kg.K$].

$C_{\varepsilon 1}$ Constant for $k-\varepsilon$ turbulence model.

$C_{\varepsilon 2}$ Constant for $k-\varepsilon$ turbulence model.

C_μ Constant for $k-\varepsilon$ turbulence model.

D Kinematic diffusivity.

D_{eff} Effective kinematic diffusivity.

d_p Diameter of the particle, [kg/m^3].

F_1 Blending function for SST turbulence model.

F_2 Blending function for SST turbulence model.

g Gravitational acceleration, [m/s^2].

h Enthalpy, [m^2/s^2].

h Heat transfer coefficient, [$W/m^2.K$].

K Thermal conductivity, [$W/m.K$].

K_{eff} Effective thermal conductivity, [$W/m.K$].

k Turbulence kinetic energy, [m^2/s^2].

m_p Mass particle, [kg].

m_t Tracer mass, [kg].

p Pressure, [N/m^2].

Pr Turbulent Prandtl number.

P_k Turbulence production, [$kg/m.s^3$].

Re Reynolds number.

S Invariant measure of the strain rate.

S_c Turbulent Schmidt number.

Q Total volumetric flow rate through the tundish, [m^3/s].

Q_a Volumetric flow rate through the active region, [m^3/s].

q'' Heat flux, [W/m^2].

$\dot{q}$ Volumetric flow rate, [m^3/s].

T Temperature, [K].

T_{ref} Reference temperature, [K].

T_∞ Room temperature, [K].

t Theoretical residence time, [s].

t_{min} Minimum residence time, [s].

t_{peak} Maximum residence time, [s].

U_j Fluid velocity, [m/s].

U_p Velocity particle, [m/s].

V Tundish volume, [m^3].

V_D Dead volume.

V_M Well-mixed volume.

V_P Dispersed plug volume.

α_3 Constant for SST turbulence model.

β Thermal expansion coefficient, [K^{-1}].

β' Constant for SST turbulence model.

β_3 Constant for SST turbulence model.

ε Emissivity.

ε Turbulence eddy dissipation, [m^2/s^3].

θ Dimensionless residence time.

θ_{min} Dimensionless minimum residence time.

θ_{peak} Dimensionless maximum residence time.

$\overline{\theta}$ Dimensionless mean residence time.

$\overline{\theta}_C$ Dimensionless mean time from $\theta = 0$ to $\theta = 2$.

μ Dynamic viscosity, [$kg/m.s$].

μ_{eff} Effective viscosity, [$kg/m.s$].

μ_t Turbulent viscosity, [$kg/m.s$].

ν Kinematic viscosity, [m^2/s].

ν_t Turbulent viscosity, [m^2/s].

ρ Fluid density, [kg/m^3].

ρ_p Density of the particle, [kg/m^3].

ρ_{ref} Reference density, [kg/m^3].

σ Stefan-Boltzmann constant.

σ_k Constant for $k-\varepsilon$ turbulence model.

σ_{k3} Constant for SST turbulence model.

σ_ε Constant for $k-\varepsilon$ turbulence model.

$\sigma_{\omega 3}$ Constant for SST turbulence model.

ω Turbulence frequency, [m^2/s^2].

CONTENTS

1 INTRODUCTION

The continuous casting process transforms the liquid metal into a solid. In contrast to conventional form of steelmaking, where the molten steel is poured into a closed mold, which causes the interruption of the process every time the mold is completed, the continuous casting process occurs in a continuous basis; this is possible owing to the use of an opened mold.

The continuous casting process has many advantages over the traditional one, such as higher quality and higher productivity of molten metal, which gives it preference when low cost and high efficiency are sought in industry. Therefore, these advantages make this process the most used technique to produce steel currently. Fig. 1.1 illustrates the worldwide growing development of steel produced by continuous casting process.

Figure 1.1 – Fraction of steel produced by continuous casting process in the last decades.

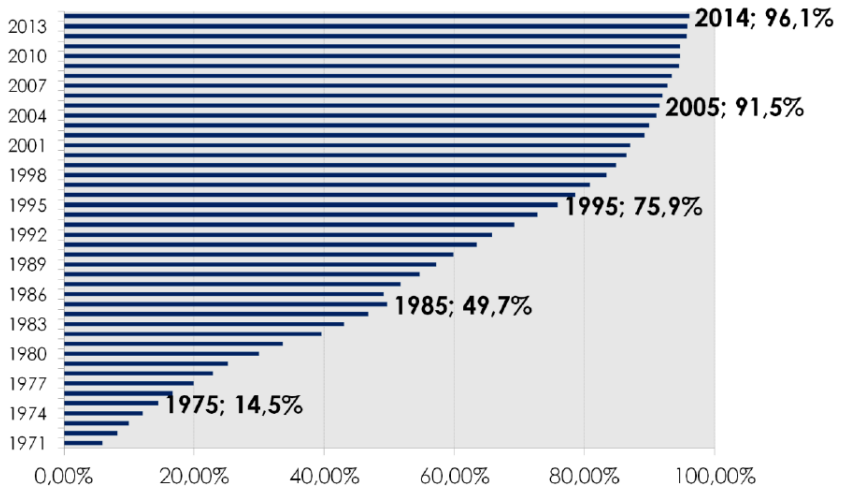

Source: World Steel Association (2015).

As can be seen from Fig. 1.1, nowadays continuous casting process is responsible for producing over 96% of steel in the world. Accordingly, the full comprehension about what happens into the main devices being part of this process is of vital importance to further design and optimize it.

In order to attain steel cleanliness, one of the most important component devices employed in continuous casting process is the so-called tundish. In the last decades, the tundish has been designed to be not only an intermediate vessel between the ladle and the mold, but also an inclusion removal and a metallurgical reactor. In addition, it has the important function

to maintain the ladle exchange without interrupt the process and to keep the liquid metal's height into the mold constant.

With the aim to increase the steel quality, some flow control devices have been added to the tundish, and therefore the flow pattern may change. The most common flow modifiers include dams, weirs, stopper rods, turbulence inhibitors, baffles, and gas injectors.

Considering the importance of liquid steel to metallurgy industry, several researchers have carried out investigations in both experimental and numerical area, concerning the main relevant aspects that govern the fluid flow and heat transfer into the tundish (Gardin et al., 2002; Kumar et al., 2004). As we know, experimental analysis has many drawbacks, such as high cost of equipment and less possibility to both change and analyze different scenarios. On the other hand, performing numerical analysis of continuous casting processes can overcome these drawbacks.

The long-stablished methods to solve the partial differential equations numerically can be divided into three main categories: Finite-Volume Method (FVM), Finite Element Method (FEM), and Finite Difference Method (FDM). Moreover, Finite-Volume Method is the most used method in the commercial packages, since it is the only approach that can warrant local conservation of the physical quantities (mass, momentum, and energy) (Maliska, 2004).

Based on numerical approaches, Computational Fluid Dynamics (CFD) can be defined as the analysis of systems that involve fluid flow, heat transfer, and related phenomena such as combustion processes. In addition, solution is obtained in a computer-based simulation. CFD is based on the approximate solution of governing equations, viz., mass, momentum, and energy equations along with proper initial and boundary conditions. Also, CFD has gained great attention in the research community as a result of its flexibility and high cost-effective processes.

To perform a CFD simulation, four main steps must be followed:

- Defining the geometry and creating the mesh;
- Defining the physical model;
- Solving the given CFD problem;
- Visualizing the obtained results.

Ansys CFX, which is built under CFD approaches, combines an advanced solver with pre and post-processing powerful tools. Moreover, it consists of four software modules that take a geometry and a mesh from an external program, and pass the information required

to perform a CFD analysis. To discretize the transport equations, the Element-based Finite-Volume Method (EbFVM) is used.

Analyzing the various physical and geometric parameters involved in tundish modeling might be a complex task, especially when experimental techniques are applied. However, CFD gives rise to an easier way to deal with this task by combining numerical and computational tools. There are many advantages when comparing CFD techniques with experimental approaches, for instance, reduction of time to analyze systems with no added expenses, possibility to perform studies under hazardous conditions, infinite level of parametric studies leading to unlimited possibilities, reliable results, and ability to simulate ideal and realistic relevant problems. Nevertheless, to take full advantage of CFD capabilities, experience and exhaustive trial-and-error analysis is required by the design engineer.

However, numerical simulation in steel continuous casting tundishes should not replace experimental analysis, instead, numerical analysis must complement it in order to make integrated analysis in complex systems of vital importance to engineering.

1.1 OBJECTIVES

1.1.1 *General objective*

The main objective of this study is to evaluate qualitatively and quantitatively the flow field and heat transfer within a steel continuous casting tundish of a local steelmaker company.

1.1.2 *Specific objectives*

The main objective may be split into the following specific objectives:

- Assess the velocity and temperature fields into the tundish;
- Through RTD (Residence Time Distribution) analysis, estimate time parameters (minimum and mean residence times) and the proportions of dead, dispersed plug, and well-mixed volumes;
- Estimate the proportion of removed non-metallic inclusions at slag layer;
- Validate the numerical methodology using experimental works from the literature;

- Evaluate the influence of flow modifiers (that is, dams and weirs) upon the liquid steel flow and their efficiency in making the liquid steel cleaner.

1.1.3 *Structure of the present work*

In the present work, a numerical modeling of a steel continuous casting tundish was performed. Eulerian and Lagrangian based analysis using both isothermal and non-isothermal models were studied. Also, two turbulence models, namely, the $k-\varepsilon$ model (Launder and Spalding, 1974) and SST model (Menter et al., 2003), were tested. The remainder of this work is divided in the following chapters.

Chapter 2 provides a literature study, where a detailed analysis of the relevant aspects concerning tundish modeling is presented.

Chapter 3 briefly describes the work methodology, showing each step developed in the present study.

Chapter 4 shows the mathematical model for obtaining the flow field, heat transfer, and particle path into the tundish. Also, initial and boundary conditions are shown.

Chapter 5 presents important considerations, such as physical and operating parameters, main assumptions, and solution procedure.

Chapter 6 provides the results obtained in the simulations along with some discussions of the results.

Finally, chapter 7 presents the conclusion of this work and suggestions for future work.

2 LITERATURE STUDY

2.1 The continuous casting process

The continuous casting process was conceived by Henry Bessemer in the 19th century. However, this process became widespread in 1960s only (Thomas, 2001b). The aforementioned process has not only been used to produce steel worldwide, but also some other basic metals have made use of it, including aluminum, copper, and nickel.

The main components of continuous casting machine, which are shown in Fig. 2.1, are listed below:

- Ladle;
- Tundish;
- Mold;
- Support rolls;
- Cooling spray nozzles.

Figure 2.1 – Schematic of steel continuous casting process.

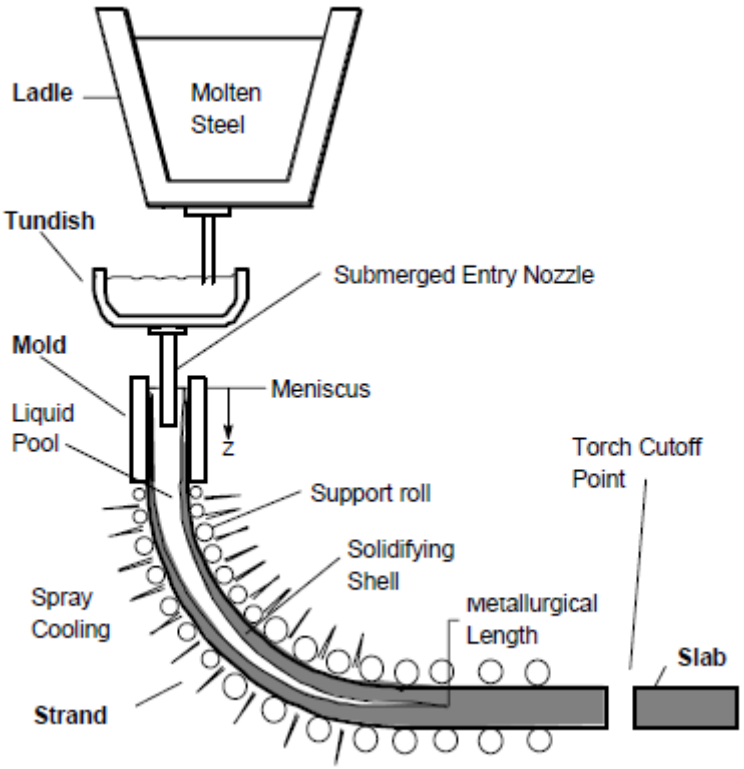

Source: Thomas (2001a).

According to Thomas (2001b), this process is described as follows: The steel, previously melted in a furnace is poured into a ladle. Then, molten steel is brought into the tundish through a shroud. The tundish distributes the liquid steel through the submerged entry nozzle into the mold. To protect against undesirable oxidation due to exposure to air, a slag layer is kept on the top of liquid steel of all vessels. Also, the nozzles used between the ladle, tundish, and mold need to be protected through the use of ceramic materials. In the mold, which is water-cooled, the solid shell begins to form. Drive rolls, running at a constant rate remove the solid shell from the mold. Furthermore, rolls must protect the solid steel from ferrostatic pressure. Water-air mixture sprays cool the strand surface to reduce its temperature until the steel core is fully solidified. Finally, reaching the metallurgical length, steel solidification is completed and the strand can be cut into slabs by making use of a torch.

The present work focus only on tundish; since this continuous casting component it is considered to be the last chance to make the steel cleaner before the solidification begins. In addition, it serves as a refining vessel to float out inclusions into the slag cover (Chakraborty and Sahai, 1992).

2.2 The steel continuous casting tundish

As previously pointed out, tundish plays a relevant role in continuous casting process. Its role has evolved from a simple reservoir to being a grade separator, an inclusion removal device, and a metallurgical reactor. Several tundish designs have as their aim the change in flow patterns to either achieve minimum mixed-grade length during grade transition or to increase inclusion particle removal at the slag layer (De Kock, 2005).

Once inclusion particles remain into liquid steel, they may produce local internal stress concentration, which would cause reduction in the steel fatigue life (Thomas, 2001b). As an alternative to the traditional used flow modifiers, such as dams and weirs to obtain inclusion removal, some authors have proposed the use of gas injection to improve the entrapment of non-metallic inclusions by slag layer (Jun et al., 2008; Kruger, 2010; Mendonça, 2016).

Direct measurements in industrial plants are a hard task to do, especially due to the operating conditions, such as high temperature, and high opacity (poor flow visualization). Thus, physical and mathematical modeling seem to be more plausible ways to analyze the flow field and heat transfer into steelmaking tundishes.

Even with enormous amounts of results that can be obtained by numerical modeling studies, they are practically useless without validations. Therefore, to provide confidence on numerical results, physical modeling studies must be carried out.

In order to represent the fluid flow of molten steel into tundish through experimental analysis, reduced or full-scale water models can be used. Nonetheless, for truly characterize the fluid flow, some conditions of similarities between the model and the actual tundish need to be satisfied. The similarities are divided into geometric, mechanical, chemical, and thermal ones.

In an aqueous reduced scale model, geometrical and mechanical similarities must be attempted. To meet geometrical similarity, all dimensions must obey a specific relation between scaled model and actual tundish, whereas mechanical similarity is achieved by keeping the same forces on model and actual tundish through the Froude number (inertial forces/gravitational forces), since it is difficult to maintain both Reynolds (inertial forces/viscous forces) and Froude similarities (Kemeny et al., 1981; Sahai and Ahuja, 1986). In addition, as stated by Mazumdar (2013), when non-isothermal flows are under study, Richardson number (thermal buoyancy/inertial forces) needs also to be considered.

Reduced or full-scale water models have been used to assess crucial phenomena within the tundish. Water at 20ºC and liquid steel at 1600ºC have similar kinematic viscosities (dynamic viscosity/density), and hence make possible that important conclusions can be drawn from devices using water. Table 2.1 shows that kinematic viscosity of both fluids is of the same order of magnitude.

Table 2.1 – Physical properties of water at 20ºC and liquid steel at 1600ºC.

	Water	Liquid steel
Dynamic viscosity (Pa.s)	0,001	0,0064
Density (kg/m^3)	1000	7014
Kinematic viscosity (m^2/s)	1.10^{-6}	$0,913.10^{-6}$

Source: Kemeny et al. (1981).

Gardin et al. (2002) performed both experimental and numerical studies, evaluating turbulence through the measurement of mean and fluctuating velocity using Laser Doppler

Anemometer (LDA) to determine the flow field into the tundish, thus forming the basis for a numerical model validation.

Through a wide range of design and operating parameters (tundish width, bath height, inlet-exit distance, inlet Froude number, tundish flow rate), Singh and Koria (1993) studied the molten steel fluid flow phenomena using a perspex glass water model. In this study, they found out that the proposed correlations were able to predict the fluid flow into the tundish very well, therefore, proper modifications could be proposed to existing devices and select optimal parameters to a new tundish.

2.3 Non-metallic inclusions

Non-metallic inclusions (mainly formed by oxides, sulfides, and nitrides), which arise from steel continuous casting process can be called as endogenous and exogenous. Endogenous inclusions are originated from deoxidation of products or precipitation of inclusions during cooling and solidification of steel. On the other hand, exogenous inclusions are formed through chemical reaction (reoxidation) and mechanical interaction among liquid steel, slag layer entrainment and lining refractory erosion (Zhang and Thomas, 2003).

In the steel continuous casting process, the level of steel cleanliness depends on the desired end products. Therefore, a maximum inclusion size is acceptable for specific steel products provided that this will not affect their final application. The maximum inclusion size for some steel products is shown in Table 2.2 (Zhang and Thomas, 2003).

Table 2.2 – Steel cleanliness requirements for maximum inclusion size.

Steel Product	Maximum inclusion size (μm)
Automotive industry	100
Pipelines	100
Wires	20
Ball bearings	15
Tire cords	10

Source: Adapted from Zhang and Thomas (2003).

Non-metallic inclusions do not pose any trouble for steel cleanliness if they stay as small as 1 μm (Ishii et al., 2001). However, owing to intrinsic mechanisms of collision and coagulation, they can become larger, and consequently may cause severe damages to the final product.

Amongst the several aspects that present vital influence over the mechanical behavior of steel, the size distribution is intrinsically important since larger inclusions are the most harmful to mechanical properties. As stated by Zhang and Thomas (2003), inclusions may reduce ductility, fracture toughness, corrosion resistance, hydrogen resistance to induced cracks, among others.

As non-metallic inclusion density has about half value of liquid steel density, they can be removed at the slag cover when they reach it by flotation mechanism. Therefore, the requirements for steel cleanliness can be satisfied. To achieve this, inclusions must stay into the tundish as much as possible in order to have enough time for them to float out. Therefore, steel makers have been making use of flow control devices to change the flow pattern into the tundish, to promote inclusion flotation, and to remove them by the slag layer.

2.4 Flow control modifiers

Fulfilling the clean steel requirements by substituting the existing tundish geometry is not always an economical task, hence the molten steel flow into the tundish may be altered through the use of flow control modifiers. The most common fluid flow modifiers include dams, weirs, stopper rods, turbulence inhibitors, baffles, and gas injectors. In the last decades, many authors have performed both experimental and numerical studies including such devices into the tundish, in order to improve the steel cleanliness (Wollmann, 1999; Kumar et al., 2004; Bensouici et al., 2009; Wang et al., 2015). Fig. 2.2 shows a typical tundish with dams and weirs, which are also the flow control devices used in the present work.

Figure 2.2 – Flow control modifiers (dams and weirs).

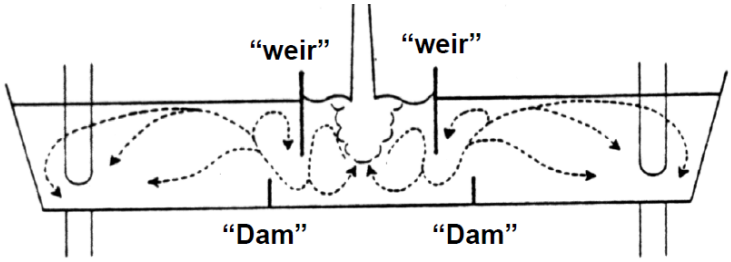

Source: Kemeny et al. (1981).

The weir can be thought of as a partial wall extending from the surface of molten steel to a certain level above the tundish bottom; on the other hand, the dam can be defined as a partial wall extending from the tundish bottom to a level below the slag cover.

According to Sahai and Ahuja (1986) the weir can guarantee low intensity of turbulence at slag slayer; however, it cannot eliminate short circuiting in a given tundish. Unlike the weir, dam can eliminate short circuiting completely, and besides this it has some others desired features such as the creation of surface directed flows, the increase in the mean residence time, and the trap of higher turbulent velocity values at the inlet region.

In the work of Bensouici et al. (2009), the position of flow control devices (dams and weirs) into the tundish was studied. It was concluded that these devices can promote floatation of non-metallic inclusions due to the above explanation. Some of their results are illustrated in Fig. 2.3.

Figure 2.3 – Typical RTD (Residence Time Distribution) curves for different tundish configurations.

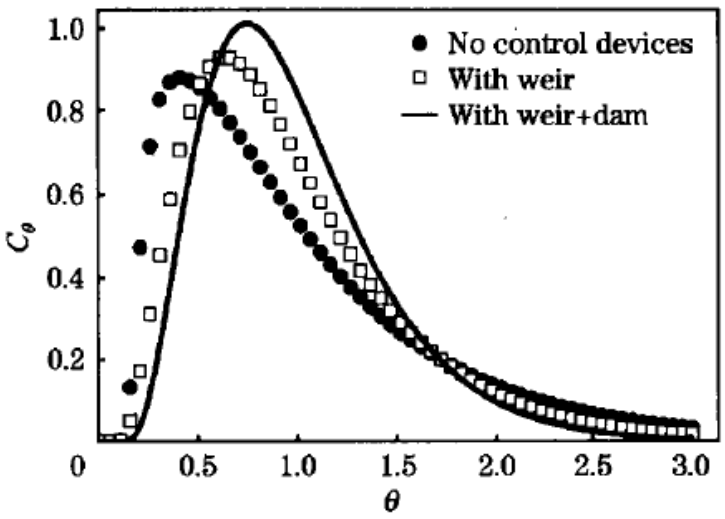

Source: Bensouici et al. (2009).

Kemeny et al. (1981) performed experimental analysis into tundishes with no flow modifiers and also tested two different configurations, namely, one with dam only and another with dam and weir acting as flow modifiers. The authors evaluated the best location for the flow control devices through the analysis of characteristic times provided by RTD curves. A better tundish performance was found when the flow modifiers were inserted.

Wollmann (1999) tested four different types of flow modifiers in a physical analysis of a T-delta-shaped tundish, and he concluded that even with the simplest configuration of flow control device (using just one dam), an increase in mean residence time and elimination of short-circuiting could be observed.

Finally, it is worth noting that, in most of the times, the desired end results are made possible by making use of a combination of the aforementioned flow control devices, then, promoting higher rates of inclusion removal for a given tundish, and therefore to make the steel cleaner.

2.5 Thermal analysis applied to tundish modeling

Many studies have been carried out under isothermal conditions. However, non-isothermal fluid flow should be taken into account when actual tundishes are modeled, since temperature variation occurs from the inlet to the outlet of stream by heat losses to the atmosphere through walls and slag layer surface.

According to Sheng and Jonsson (1999), inside the tundish owing to low average flow velocity and high superheated temperature, there is a thermal buoyancy force that cannot be neglected and consequently, a thermal stratification will always exists inside the tundish.

As turbulence is decreased from inlet to the bulk fluid region, buoyant forces become predominant and hence natural convection plays an important role in the floatation of non-metallic inclusions in these regions (Ray, 2009). The non-isothermal behavior of molten steel into the tundish may cause significant changes in the mean residence time, temperature distribution, and inclusion movements (Sheng and Jonsson, 1999). Therefore, final products can be directly influenced by the non-isothermal field into the tundishes.

De Kock (2005) performed both a plant trial and a water model study in conjunction with numerical analysis in various types of tundishes. He aimed to obtain RTD curves as well as temperature distribution in non-isothermal tundishes, in order to achieve an optimum design for each configuration. One of his results can be seen in the following figure, where temperature variation throughout the domain is shown.

Figure 2.4 – Temperature contour on longitudinal plane.

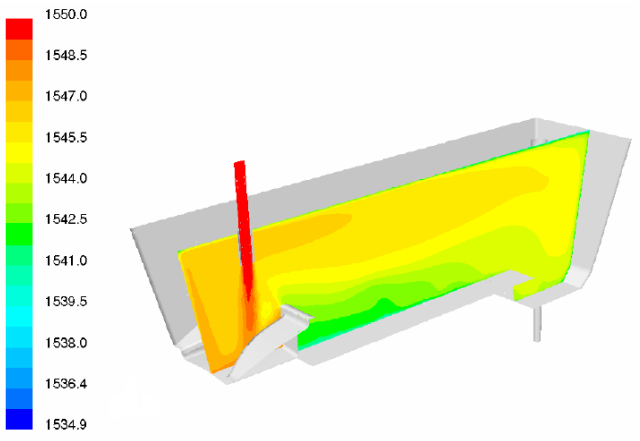

Source: De Kock (2005).

In addition, in accordance with the above-mentioned study, Ray (2009) stressed out that in most of the studies in the literature, the temperature difference between the ladle shroud and the tundish outlet assumes values in the range of 15ºC to 25ºC.

Alizadeh et al. (2008) carried out a steady state water modeling analysis under non-isothermal conditions in a twin-slab-strand continuous casting tundish. Their results showed that RTD curves were completely different under isothermal and non-isothermal conditions as can be seen in Fig. 2.5. Also, they related this divergence due to the presence of mixed convection phenomena in the non-isothermal tundish.

Figure 2.5 – Comparison between isothermal and non-isothermal RTD curves.

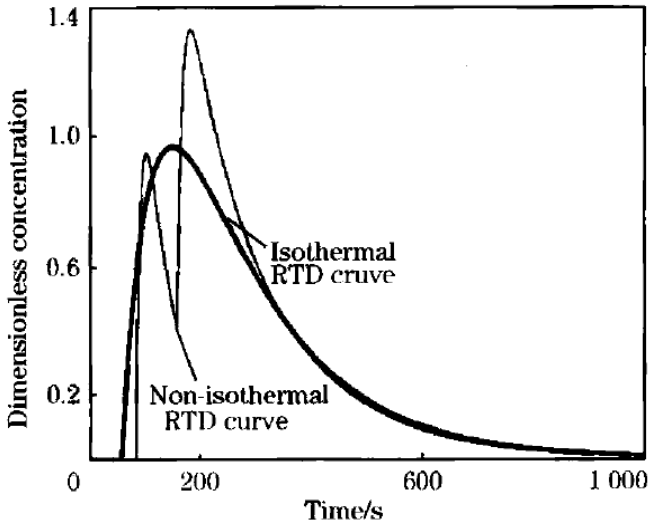

Source: Alizadeh et al. (2008).

The present study considered the heat losses through the slag layer and walls only by radiation and convection heat transfer. The main mechanism of heat losses to the surroundings is found to be the radiation heat flux, since the latter mechanism is directly proportional to the fourth power of liquid steel temperature, while the convection heat losses are proportional to only the first power of molten steel temperature (Joo et al., 1993; Incropera and DeWitt, 1990). The summation of the aforementioned heat losses (energy/(area*time)) to the surroundings can be obtained by the following expression:

$$q'' = h\left(T - T_\infty\right) + \sigma\varepsilon\left(T^4 - T_\infty^4\right), \tag{2.1}$$

where q'' denotes the total rate of energy per unity of superficial area of the tundish, h is the heat transfer coefficient by convection, T is the wall temperature (slag layer or tundish walls), T_∞ is the room temperature, σ is the Stefan-Boltzmann constant (5.67×10^{-8} W/m^2.K^4), and ε is the material emissivity.

Generally, tundishes without any flow modifiers lose a significant amount of heat through their boundaries and hence the spatial temperature becomes nonuniformly. When adding some kind of flow control, the heat loss is reduced and then the temperature field must be more uniform (Szekely and Ilegbusi, 1989).

Miki and Thomas (1999) developed mathematical models to predict the removal of non-metallic inclusions from liquid steel in a continuous casting tundish (Al_2O_3 to be more specific). They included thermal buoyancy forces in order to calculate the temperature distribution throughout the given tundish. Fig 2.6 depicts the fraction of inclusion cluster removed considering an isothermal and a non-isothermal model. From this figure, it is possible to note that thermal convection promotes inclusion removal especially for small inclusions.

Figure 2.6 – Inclusion removal for isothermal and non-isothermal models.

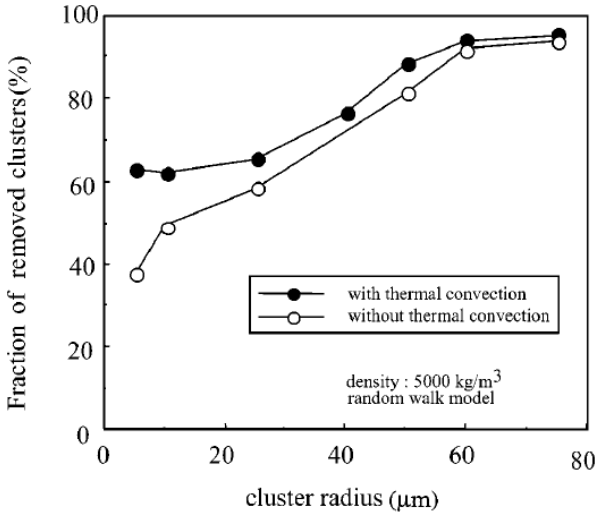

Source: Miki and Thomas (1999).

Raghavendra et al. (2013) also studied the influence of thermally induced flows for inclusion flotation. The well-known open source CFD code, OpenFOAM, was used for modeling inclusion path in a four-strand asymmetric billet caster tundish. They obtained different fractions of removed particles when comparing isothermal and non-isothermal cases. However, different from the work of Miki and Thomas (1999), flows with buoyancy forces showed lesser separation efficiency for small particles at slag layer. The two works presented agreement with each other when large inclusion removal was considered.

2.6 Numerical methods applied to tundish modeling

Solving the Navier-Stokes equations analytically is only possible for a few simplified problems such as the fully developed Couette flow. When one deals with real flows, numerical methods must be used. Basically, by using a numerical approach the set of partial differential equations are transformed into a set of algebraic approximated equations.

One knows that any numerical procedure that obtain their approximate equations through a material balance is a finite-volume method. Thus, there are different types of the aforementioned method. One of them is the Element-based Finite-Volume Method (EbFVM), denomination suggested by Maliska (2004).

Ansys CFX uses the Element-based Finite-Volume approach. In this approach the physical domain is divided into elements, and then each element is subdivided into sub-

elements according to the number of nodes of each element. In general, each sub-element is called sub-control volume because the conservation equations are integrated in time and space for each sub-element. After the integration process, the equation of each control-volume is assembled visiting all sub-control volumes that share the same node. Due to its conservative aspect, conservation of properties is guaranteed at each finite control volume.

Ansys CFX deals with three-dimensional meshes; the mesh can be composed of either hexahedral, tetrahedral, prism, and pyramid elements, or a combination of these elements. Nonetheless, for the sake of simplicity, a two-dimensional mesh, which is constructed with triangle and quadrilateral elements is described in Fig. 2.7. In this Figure, the blue numbers represent the elements, the sub-control volumes are represented by the SVC_i and, the control volume related to the vertex 5 is described by green area. In general, hybrid meshes (combination of different elements) are used to better capture the physical phenomena of the problem to be solved. This approach has been successfully applied in several fields, see for instance, Marcondes and Sepehrnoori (2010), Pimenta (2014), and Filippini et al. (2014).

Figure 2.7 – Unstructured mesh and control-volume.

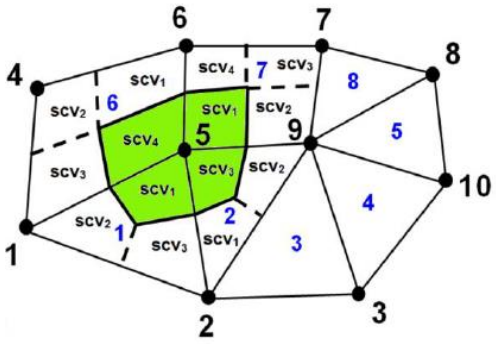

Source: Fernandes (2014).

During the process, all variables and material properties are stored at the nodes. Joining the edge centers and element centers, a control volume is then constructed around each node. This is called median dual method (Ansys CFX, 2011), and gives rise to a cell-vertex approach.

During the integration of transport equations volume integrals arise, which are described as function of the mean property values within the control volume. Moreover, surface integrals are generated by the summation over each face of the volumes associated with integration points (Kruger, 2010). In order to associate values at integration points with variables stored at nodes, interpolation functions are used.

Diffusion terms do not pose numerical instabilities when interpolation schemes are applied to interpolate physical properties from the nodes to the integration points (owing to their elliptic behavior); on the other hand, care should be taken when advective terms are involved. The use of non-exact interpolation functions gives rise to truncation errors. When these errors are associated with advective terms, numerical oscillation and numerical diffusion errors are yielded (Maliska, 2004).

To achieve physically realistic numerical results, interpolation schemes must possess fundamental properties. The most relevant ones are conservativeness, boundedness and transportiveness (Versteeg and Malalasekera, 2007).

2.7 Turbulence Models

When fluid flows are controlled by viscous diffusion of vorticity and momentum, they are called laminar flows, and the Reynolds number is in general small. As Reynolds number increases, the inertia terms overcome the viscous stresses, and consequently rapid velocity and pressure fluctuation appear in the fluid flow and the motion becomes inherently three-dimensional and unstable, which can be described as a turbulent flow (Wilcox, 2006).

Turbulent eddies, which can be thought of as a local swirling motion where the vorticity can often be very intense, appear in a wide range of sizes and permit mixing and effective turbulent stresses to come up. Turbulence is mainly dominated by larger eddies as highlighted by Wilcox (2006).

The unsteady Navier-Stokes equations are capable of computing the smallest length and time scales of turbulence. However, these calculations are not feasible in terms of computing resources, since temporal and spatial grids need to be sufficiently fine in order to resolve all turbulent scales. Besides, for practical engineering applications the assessment of smaller eddies when compared to the larger eddies are not important.

There are three major numerical methods for predicting turbulent flow: Direct Numerical Simulation (DNS), Large Eddy Simulation (LES), and Reynolds Averaged Navier-Stokes (RANS). DNS is the most accurate method for solving Navier-Stokes equations and it is worth to mention that it can be thought of as the easiest method to implement. However, it will depend on computational resources that will not be available in most research centers around the world. In addition, the DNS solves all scales of the flow. By solving the smallest turbulence scales, DNS is regarded as a highly costly computational approach, so this method

is not practicable for modeling actual 3D turbulent flow in tundishes (Omranian, 2007; Chattopadhyay et al., 2010).

By using the LES approach, the large scale quantities are fully solved while the small scales are modeled. A spatial filtering approach separates the resolved turbulent scales from the modeled ones. LES is less accurate than DNS, however, it is numerically more economic (Argyropoulos and Markatos, 2015). Gardin et al. (2002) used an RNG subgrid-scale LES model, which is available in the commercial software FLUENT, to perform numerical analysis for a given tundish. Even though the agreement with experimental results were not good and convergence time took so long, they concluded that through the adjustment of some constants, the LES model can work both for the jet spreading and the wall jet predictions.

RANS is based on averaging the equations of motion resulting in a set of partial differential equations. In spite of having some limitations, due to the averaging process, to date the RANS models are still the first choice when numerical tundish modeling is required.

When averaging mass and momentum equations, additional terms appear and therefore this form a non-closed set of equations. These new terms are called Reynolds stresses, and as a result of this further information is necessary to balance the equations and the unknowns. Turbulence models are responsible for computing Reynolds stresses, and then close the system of mean flow equations in order to make the solution possible.

Commonly, RANS turbulence models are grouped into classes based on the number of additional transport equations that need to be solved together with the mean flow equations (Versteeg and Malalasekera, 2007). Table 2.3 presents the number of additional variables for each turbulence model.

Table 2.3 – Turbulence models.

No. of extra transport equations	**Turbulence Model**
Zero	Mixing Length Model
One	Sparlat-Allmaras Model
Two	k-ε Model
	k-ω Model
	Algebraic Stress Model
Seven	Reynolds Stress Model

Source: Versteeg and Malalasekera (2007).

The fluid flow into the tundish is promoted by the nozzle that is placed at the exit of the ladle. At the inlet region (and also at outlet) of the tundish the flow regime is mostly turbulent, while far from the inlet (bulk region), turbulence decreases progressively, and hence inclusions can be removed (Gardin et al., 2002).

Accuracy is most required at inlet region in order to analyze correctly both the spreading rates of the jet and impinging wall boundary layer, consequently a local refined grid in conjunction with a good turbulence model need to be used (Gardin et al., 2002).

It is observed that two-equation models are the first ones preferred by industry. Also, two-equations eddy viscosity models are still preferable for CFD calculations, with the standard $k-\varepsilon$ model (Launder and Sharma, 1974) and $k-\omega$ model (Wilcox, 1988) being the most widely used. Researchers have applied $k-\varepsilon$ model exhaustively for the tundish modeling and this model is currently considered to be well tested. Also, good agreements with experimental studies have been achieved with the application of this model.

The tundish metallurgy area has been following this tendency since $k-\varepsilon$ model has been massively employed over the years by many authors to account for turbulence quantities (Yeh et al., 1994; Daoud, 2006; Tiang-peng et al, 2012; Alves, 2014).

Despite of being exhaustively used, according to Ilegbusi (1994), $k-\varepsilon$ turbulence model has some tendency to overestimate mixing in regions, where turbulent and laminar regimes are present; such situation often occurs in vessels like tundishes. Accordingly, each region (turbulent and laminar) of the tundish domain must be properly modeled by making use of a suitable turbulence model.

In order to figure out how turbulent quantities behave inside tundishes, several authors have performed studies analyzing different types of turbulence models. Jha and Dash (2004) studied the numerical prediction of tracer concentration at tundish outlet with six different turbulence models, namely, the standard $k-\varepsilon$, the $k-\varepsilon$ RNG, the low-Reynolds number Lam-Bremhorst model, the Chen-Kim high-Reynolds number model (CK), the Chen-Kim low-Reynolds number model (CKL), and the simplest constant effective viscosity model (CEV). Gardin et al. (2002) used the $k-\omega$ model, three types of low-Reynolds number $k-\varepsilon$ model variants, and the RNG sub-grid scale model (LES-model) to take into account the viscous damping away from the walls. The analysis showed that both the $k-\omega$ model and the LES model did not produce good agreement with experimental measurements whereas the $k-\varepsilon$ variants proved to be very successful.

More advanced turbulence models have been proposed, one of them is the Shear Stress Transport (SST) model, which combines the advantages of both $k-\varepsilon$ and $k-\omega$ model. SST activates $k-\omega$ model in the near-wall region and the $k-\varepsilon$ model for the remainder of the flow (Menter et al., 2003). Kruger (2010) suggested the use of SST model due to the above explanations, and indeed good results were achieved by him.

Taking into account the above explanations, the $k-\varepsilon$ turbulence model was employed in the present study for some simulations in order to test its efficiency in modeling the fluid flow phenomena in tundishes. However, most simulations, including fluid flow, heat transfer, and Lagrangian analysis were made by making use of the SST turbulence model.

2.8 RTD (Residence Time Distribution) analysis

One way to assess information about fluid flow in a tundish, either numerically or experimentally, is perform a stimulus-response experiment through the injection of a tracer (non-reactive tracers are widely used) in the incoming flow and monitoring its concentration at exit. By plotting this concentration against time, one obtains the so-called Residence Time Distribution (RTD) curve or C-curve. Residence time can be defined as the time that a single fluid element spends within any vessel. This distribution curve is originated from the fact that some fluid element spend more time within the tundish than others (Mazumdar and Guthrie, 1999).

After obtaining the steady state fluid velocity in the tundish, it is possible to characterize the fluid flow in different regions (mixed or combined model). According to Sahai and Ahuja (1986) and Sahai and Emi (1996), the combined or mixed model has been quite used to the assessment of RTD curves. The mixed model characterizes the fluid flow into the tundish in three volumes: dispersed plug flow volume, well-mixed volume, and dead volume. Fig. 2.8 depicts the combined model. It is worthwhile to note that the order of the plug and well-mixed regions does not change the end C-curve.

Figure 2.8 – Combined model.

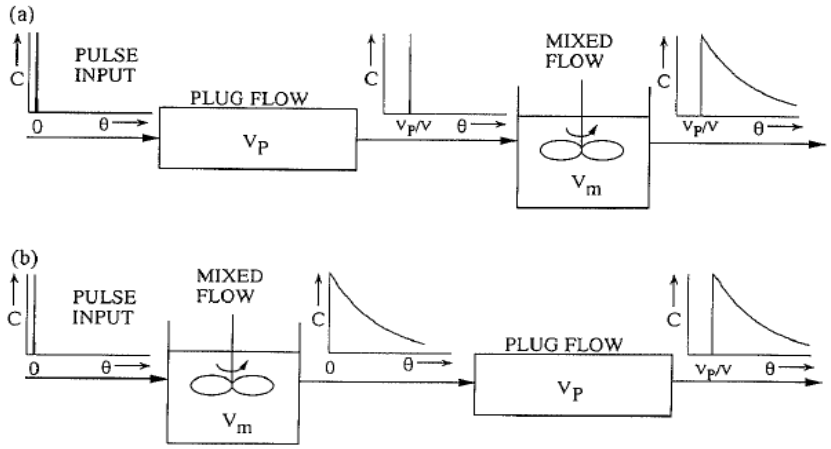

Source: Sahai and Emi (1996).

In addition, the combined model can be grouped into an active region (a combination of plug and well mixed volumes) and a dead region as can be seen in Fig. 2.9.

Figure 2.9 – Fluid flow crossing the active and dead regions in a combined model.

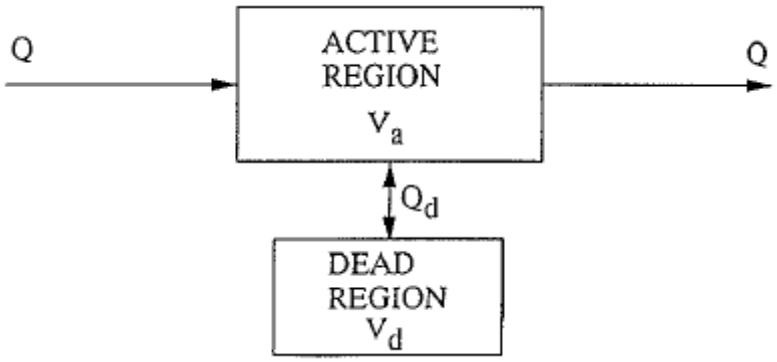

Source: Sahai and Emi (1996).

In plug flow region, there is not longitudinal mixing, but transversal mixing may occur. Furthermore, the residence time is the same for all fluid elements in the plug flow region. Unlike the plug flow region, the mixed flow region shows the maximum possible mixing. The last region that completes the model is the dead region, which can be represented by the fluid elements that move slowly and spend more than two times the mean residence time within the tundish. In addition, sometimes, there may be a kind of undesirable volume, called short-circuiting volume, which stands for a portion of the fluid volume that leaves the tundish in a brief period of time.

Having described the characteristic volumes, one notes that some important characteristic times are also worth to mention. They are defined as follows:

- Theoretical residence time, t

The theoretical residence time depends only on the geometric and operational parameters and it is obtained dividing the tundish volume, V, by the volumetric flow rate, $\dot{q}$.

$$t = \frac{V}{\dot{q}}, \tag{2.2}$$

- Minimum residence time, t_{min}

The minimum residence time can be defined as the time when the first fluid element leaves the tundish. In a tracer pulse experiment, it is represented by the first detected concentration of the tracer at the exit.

- Mean residence time

The mean residence time stands for the mean time spent by all fluid elements into a given tundish.

- Maximum residence time, t_{peak}

The maximum residence time represents the time when the maximum quantity of fluid elements leave a given tundish.

In order to avoid some external influence, such as amount of tracer mass, tundish volume, inlet volumetric flow rate, as well as to compare different kinds of tundishes, the C-curve must be put in a dimensionless form.

According to Levenspiel (1998), each dimensionless residence time, θ, is obtained dividing each instant of time, t_i, by the theoretical residence time, t, therefore, we have:

$$\theta = \frac{t_i}{t}, \tag{2.3}$$

$$\theta_{min} = \frac{t_{min}}{t}, \tag{2.4}$$

$$\theta_{peak} = \frac{t_{peak}}{t}, \tag{2.5}$$

where θ_{min} and θ_{peak} stand for the dimensionless form of the minimum and maximum residence time, respectively.

To normalize the tracer concentration, C_i, collected at the outlet of the tundish at each instant of time, the tracer mass, m_t, as well as the tundish volume, V, are related by the following expression, resulting in a dimensionless form of the concentration, C (Levenspiel, 1998):

$$C = \frac{C_i}{m_t / V}, \tag{2.6}$$

The dimensionless mean residence time is calculated through the Residence Time Distribution (RTD) curve. If the concentration at the exit is measured at equal time intervals, the dimensionless mean residence time, $\bar{\theta}$, is calculated as follows:

$$\bar{\theta} = \frac{\sum_{\theta=0}^{\infty} C_i \theta_i}{\sum_{\theta=0}^{\infty} C_i}, \tag{2.7}$$

The dead volume fraction can be calculated through the following expression:

$$\frac{V_D}{V} = 1 - \frac{Q_a}{Q} \cdot \bar{\theta}_C, \tag{2.8}$$

In the above expression, Q_a represents the volumetric flow rate through the active region and Q the total volumetric flow rate through the tundish. The term, $\frac{Q_a}{Q}$, is expressed by the area under the RTD curve from $\theta = 0$ to $\theta = 2$.

$$\frac{Q_a}{Q} = \sum_{\theta=0}^{2} C_i \Delta\theta, \tag{2.9}$$

Furthermore, $\bar{\theta}_C$ is the dimensionless mean time from $\theta = 0$ to $\theta = 2$.

$$\bar{\theta}_C = \frac{\sum_{\theta=0}^{2} C_i \theta_i}{\sum_{\theta=0}^{2} C_i}, \tag{2.10}$$

Considering that the minimum residence time, θ_{min}, and maximum residence time, θ_{peak} show different values, the fraction of plug volume is calculated as (Sahai and Ahuja, 1986):

$$V_P = \frac{\theta_{min} + \theta_{peak}}{2}, \tag{2.11}$$

Finally, all volume fractions must be equal to unit, then the well mixed volume fraction is expressed by:

$$V_M = 1 - V_P - V_D. \tag{2.12}$$

Some regions of a given tundish with and without flow modifiers are showed in Fig. 2.10. This figure emphasizes the presence of dead volume in tundish corners and the leeward side of the flow control devices (dams and weirs).

Figure 2.10 – Tundish volume regions.

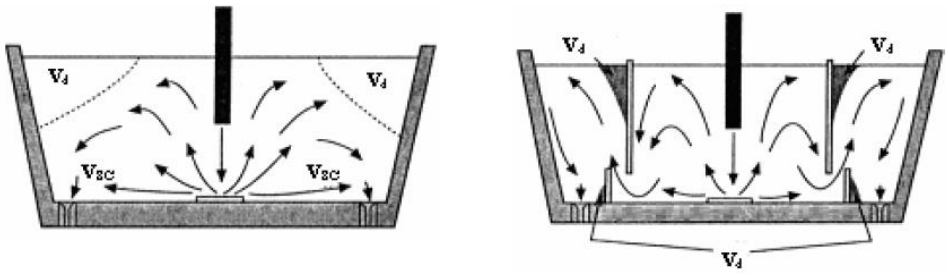

Source: Shade et al. (1996).

Furthermore, from Fig. 2.10, it is noticed that the insertion of flow modifiers (that is, dams) can make short-circuiting volume disappear (Singh and Koria, 1995).

Based on the characteristic times and volumes, the behavior of the fluid flow as well as the probability for removing non-metallic inclusions by the slag layer may be available, which can be used to propose modifications to the tundish configuration in order to improve the steel quality.

Sahai and Ahuja (1986) pointed out that to achieve maximum inclusion separation ratio in a continuous casting tundish, the following characteristics should be ensured:

- Minimum spread of residence times;
- Minimum dead volume;
- Large ratio of plug to dead volume and relatively large ratio of plug to well-mixed volume;
- Flow directed to the top surface;
- Quiescent slag layer;
- Contained regions of mixing.

The removal of non-metallic inclusions is indirectly obtained by RTD curves, therefore, in order to complement this analysis, a particle tracking analysis was also performed.

3 METHODOLOGY

The steps involved in modeling the steel continuous casting tundish using the commercial software Ansys CFX are illustrated in Fig. 3.1.

Figure 3.1 – Work methodology.

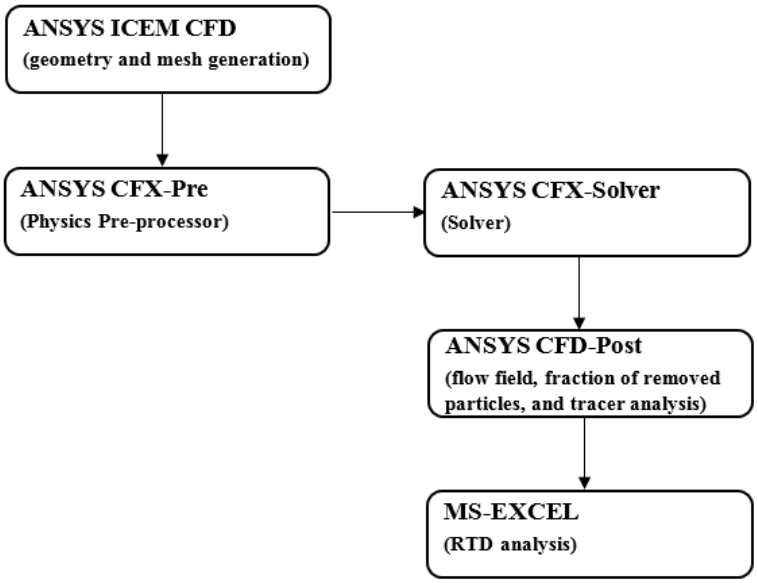

First, the geometry as well as the mesh were created using the Ansys ICEM CFD software. In the pre-processing step in Ansys CFX, the computational domain, initial and boundary conditions, working fluids (steel and water), material properties, time-steps, interpolation function, number and diameter of particles injected at inlet, steady state or transient analysis, and so on, were all defined.

The mass, momentum, energy, turbulence, tracer convection-diffusion, and particle tracking equations are solved along with initial and boundary conditions with a coupled solver using the Element-based Finite-Volume Method (EbFVM).

Finally, the results, for instance, temperature and velocity fields, fraction of removed inclusions at slag layer, were obtained by making use of the post-processor tool of Ansys CFX. In addition, minimum and mean residence time, dead volume, dispersed plug volume, and well-mixed volume, were obtained with MS-Excel.

4 MATHEMATICAL FORMULATION

The governing equations of mass, momentum, and energy were applied to compute the flow field and heat transfer within the tundish. The turbulence models have been used for calculating turbulence quantities without using Direct Numerical Simulation (DNS). For calculating the tracer concentration at the outlet tundish region a convective-diffusion transport equation was applied. Finally, in order to obtain the fraction of particles removed at slag cover, a Lagrangian tracking equation was employed.

4.1 Mass and momentum equations

In turbulent flows the instantaneous quantities, such as velocity and pressure are separated into mean and fluctuating parts, which gives rise to the well-known Reynolds Averaged Navier-Stokes (RANS) approach.

After averaging continuity and momentum equations and using the Boussinesq eddy-viscosity approximation to relate the Reynolds stresses to the strain rate of the mean motion, we obtain

$$\frac{\partial \rho}{\partial t} + \frac{\partial}{\partial x_j}\left(\rho U_j\right) = 0, \tag{4.1}$$

$$\frac{\partial}{\partial t}\left(\rho U_i\right) + \frac{\partial}{\partial x_j}\left(\rho U_i U_j\right) = -\frac{\partial p}{\partial x_i} + \frac{\partial}{\partial x_j}\left[\mu_{eff}\left(\frac{\partial U_i}{\partial x_j} + \frac{\partial U_j}{\partial x_i}\right)\right] - \rho_{ref} g \beta \left(T - T_{ref}\right), \tag{4.2}$$

where ρ is fluid density, U_j are velocity components, p is pressure, ρ_{ref} is a reference density, g is gravitational acceleration, T is temperature, T_{ref} is a reference temperature, and μ_{eff} represents the effective viscosity accounting for turbulence, which is defined by

$$\mu_{eff} = \mu + \mu_t, \tag{4.3}$$

where μ is the dynamic viscosity and μ_t is the turbulent viscosity.

For the momentum equation in the y-direction, the buoyant term is modeled by the Boussinesq model. In this model, it is assumed that density is constant, except for the buoyant term that is modeled by

$$\rho - \rho_{ref} = -\rho_{ref}\beta\left(T - T_{ref}\right), \tag{4.4}$$

in which β is the thermal expansion coefficient, expressed by the following relation:

$$\beta = -\frac{1}{\rho_{ref}}\left(\frac{\partial\rho}{\partial T}\right)_p, \tag{4.5}$$

This approximation is acceptable since the variation of the density of the liquid steel in actual processes due to the temperature difference is quite small.

4.2 Turbulence models

For modeling turbulence quantities, the two-equation $k-\varepsilon$ model as well as the SST model were used, thereby two additional variables were introduced into the system of equations.

4.2.1 *$k-\varepsilon$ turbulence model*

The $k-\varepsilon$ model assumes that the turbulence viscosity is related to the turbulence kinetic energy k and the turbulence eddy dissipation ε by the following relation:

$$\mu_t = C_\mu \rho \frac{k^2}{\varepsilon}, \tag{4.6}$$

where C_μ is a constant.

The values of k and ε are calculated via two transport equations:

$$\frac{\partial}{\partial t}(\rho k)+\frac{\partial}{\partial x_j}\left(\rho U_j k-\frac{\mu_{eff}}{\sigma_k}\frac{\partial k}{\partial x_j}\right)=P_k-\rho\varepsilon, \tag{4.7}$$

$$\frac{\partial}{\partial t}(\rho\varepsilon)+\frac{\partial}{\partial x_j}\left(\rho U_j \varepsilon-\frac{\mu_{eff}}{\sigma_\varepsilon}\frac{\partial \varepsilon}{\partial x_j}\right)=\frac{\varepsilon}{k}\left(C_{\varepsilon 1}P_k-C_{\varepsilon 2}\rho\varepsilon\right), \tag{4.8}$$

where $C_{\varepsilon 1}$, $C_{\varepsilon 2}$, σ_k, and σ_ε are constants taken from Launder and Spalding (1974). P_k is the turbulence production owing to viscous forces and it is given by

$$P_k=\mu_t\frac{\partial U_i}{\partial x_j}\left(\frac{\partial U_i}{\partial x_j}+\frac{\partial U_j}{\partial x_i}\right). \tag{4.9}$$

4.2.2 *SST turbulence model*

The two-equation SST turbulence model consists of a blending between the $k-\omega$ turbulence model near the wall and the $k-\varepsilon$ turbulence model far away from the walls. This interchange is made through a blending function F_1, which assumes a value of one near the solid surface and zero in the outer region of the flow (Menter et al., 2003). To obtain the transport equations for the turbulent kinetic energy k and the turbulence frequency ω, $k-\omega$ model is multiplied by F_1 and a modified form of the $k-\varepsilon$ model is multiplied by $1-F_1$ (Ansys CFX, 2011), resulting in the following equations:

$$\frac{\partial}{\partial t}(\rho k)+\frac{\partial}{\partial x_j}\left(\rho U_j k\right)=\frac{\partial}{\partial x_j}\left[\left(\mu+\frac{\mu_t}{\sigma_{k3}}\right)\frac{\partial k}{\partial x_j}\right]+P_k-\beta'\rho k\omega, \tag{4.10}$$

$$\frac{\partial}{\partial t}(\rho\omega)+\frac{\partial}{\partial x_j}\left(\rho U_j \omega\right)=\frac{\partial}{\partial x_j}\left[\left(\mu+\frac{\mu_t}{\sigma_{\omega 3}}\right)\frac{\partial \omega}{\partial x_j}\right]+(1-F_1)2\rho\frac{1}{\sigma_{\omega 3}\omega}\frac{\partial k}{\partial x_j}\frac{\partial \omega}{\partial x_j} \tag{4.11}$$

$$+\alpha_3\frac{\omega}{k}P_k-\beta_3\rho\omega^2,$$

where σ_{k3}, $\sigma_{\omega 3}$, α_3, $\beta^{'}$, β_3 are constants taken from Menter et al. (2003). The blending function F_1 is based on the distance to the nearest wall y as well as the flow variables, and it is calculated as follows:

$$F_1 = tanh\left(arg_1\right), \tag{4.12}$$

with:

$$arg_1 = min\left(max\left(\frac{\sqrt{k}}{\beta^{'}\omega y}, \frac{500\nu}{y^2\omega} \right), \frac{4\rho k}{CD_{k\omega}\sigma_{\omega 2} y^2} \right), \tag{4.13}$$

where ν is the kinematic viscosity (dynamic viscosity/density) and:

$$CD_{k\omega} = max\left(2\rho \frac{1}{\sigma_{\omega 3}\omega} \frac{\partial k}{\partial x_j} \frac{\partial \omega}{\partial x_j}, 1.0x10^{-10} \right). \tag{4.14}$$

Therefore, the turbulent viscosity is calculated from:

$$\nu_t = \frac{a_1 k}{max\left(a_1\omega, SF_2\right)}, \tag{4.15}$$

where

$$\nu_t = \frac{\mu_t}{\rho}. \tag{4.16}$$

S stands for an invariant measure of the strain rate and a_1 is a constant taken from Menter et al. (2003). The blending function F_2 is given by:

$$F_2 = tanh\left(arg_2\right), \tag{4.17}$$

with:

$$arg_2 = max\left(\frac{2\sqrt{k}}{\beta^{'}\omega y}, \frac{500\nu}{y^2\omega}\right). \tag{4.18}$$

4.3 Thermal energy equation

Thermal energy equation is derived from the first law of thermodynamics. By assuming that the conductive heat fluxes are expressed by the Fourier's law and neglecting the radiative and viscous dissipation effects for an incompressible flow, the final form of the energy equation can be written as:

$$\frac{\partial}{\partial t}(\rho h) + \frac{\partial}{\partial x_j}(\rho U_j h) = \frac{\partial}{\partial x_j}\left(K_{eff}\frac{\partial T}{\partial x_j}\right), \tag{4.19}$$

where h is the enthalpy and K_{eff} is the effective thermal conductivity, which we may define as:

$$K_{eff} = K + \frac{C_p \mu_t}{Pr_t}, \tag{4.20}$$

where K is the thermal conductivity, C_p is the specific heat at constant pressure, and Pr_t is the turbulent Prandtl number.

4.4 Tracer convection-diffusion equation

To obtain the RTD curve, it is necessary to solve an additional conservation equation. Therefore, the tracer (which is considered to be a passive scalar) distribution all over the domain is solved through the following advection-diffusion equation:

$$\frac{\partial}{\partial t}(\rho C) + \frac{\partial}{\partial x_j}(\rho U_j C) = \frac{\partial}{\partial x_j}\left(D_{eff}\frac{\partial C}{\partial x_j}\right), \tag{4.21}$$

where C is the tracer concentration and D_{eff} is the effective kinematic diffusivity, which is defined as

$$D_{eff} = \rho D + \frac{\mu_t}{S_c}, \tag{4.22}$$

where D is the kinematic diffusivity and S_c is the turbulent Schmidt number.

4.5 Particle tracking equation

The Lagrangian analysis is used when distinguishable mass elements are easy to follow. This analysis can be applied to describe a whole flow field (considering that the flow field is composed by a large number of particles). However, following each particle by itself might be a cumbersome process. Nevertheless, the Lagrangian modeling can be used to the present work as the non-metallic inclusions are treated as a small number of particulates immersed in the fluid domain. In this formulation, the particle tracking is performed through a force balance, which are acting on each of them.

Lagrangian particle tracking method solves a transport equation for each non-metallic inclusion in order to describe their paths. The present work is based on one-way coupling interaction between liquid and solid phases, *i.e.*, the inclusion trajectories, which are calculated through the previously calculated flow field, are influenced by the flow field and the opposite do not occur.

Applying a force balance on each particle and accounting for only their drag and buoyancy forces relative to the molten steel, since they represent the main forces on the particle (Yuan and Thomas, 2005), the inclusion path can be described as follows:

$$m_p \frac{dU_p}{dt} = \frac{1}{8}\pi d_p^2 \rho C_D \left|U - U_p\right|\left(U - U_p\right) + \frac{1}{6}\pi d_p^3 \left(\rho_p - \rho\right) g, \tag{4.23}$$

where m_p denotes the mass of the particle and U_p represents the velocity of the particle. By carefully investigating the above equation, it is possible to note that is only necessary to specify the diameter d_p and the density of the particle ρ_p to perform the analysis.

The first term on the right-hand side considers the aerodynamic drag forces and the drag coefficient C_D is given as:

$$C_D = \max\left(\frac{24}{Re}\left(1+0.15\,Re^{0.687}\right), 0.44\right), \tag{4.24}$$

The particle Reynolds number is defined as follows:

$$Re = \frac{\rho\left|U - U_p\right| d_p}{\mu}. \tag{4.25}$$

The second term on the right-hand side in Eq. (4.23) accounts for the influence of buoyancy forces on the fluid due to gravitational acceleration.

In order to simulate the random effect of turbulent eddies over the inclusion trajectories, a Random Walk Model (RWM) was used. In this model, the instantaneous velocity fluctuations depend on the local level of turbulent kinetic energy and a random number distributed between -1 and 1. Further details on this model can be found elsewhere (Crowe et al., 1998; Vargas-Zamora et al., 2003).

Miki and Thomas (1999) evaluated the influence of the Random Walk Model on trajectories of inclusions. Fig. 4.1 presents the fraction of removed particles with and without the Random Walk Model for different particle densities.

Figure 4.1 – Inclusion removal with and without the Random Walk model.

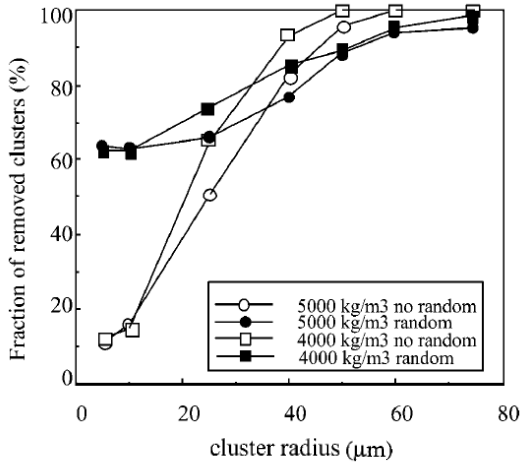

Source: Miki and Thomas (1999).

They concluded that the chaotic fluctuation due to the turbulence enhances the flotation of small inclusions. On the other hand, this random motion also causes particle collisions, then promoting a decrease in the fast removal of large inclusions.

According to Javurek (2002), if we decrease the diameter of the particle and the rising velocity towards a zero value, the particle tracking equation approaches the RTD curve model.

4.6 Initial and Boundary conditions

The present section describes all details related to initial and boundary conditions used in case studies I, II, and III. For the sake of simplicity, details concerning the validation cases were omitted. Thus, the boundary conditions, which were used for solving the steady-state analysis, are stated as follows:

- Inlet region:

At inlet, a prescribed value for normal velocity (3,57 m/s) was calculated based on the casting speed and the transverse section of a common billet produced at a local steelmaker company. These data are shown in Tables 5.2 and 5.3, which were presented in the previous section.

A prescribed value for temperature (1823K) was based upon actual operation temperature as it is also shown in Table 5.3. The turbulence intensity was set to 5% in order to account for turbulence quantities. For Lagrangian analysis, particles were injected uniformly and assuming the same value of the fluid velocity.

- Outlet region:

At the exit nozzle, a prescribed value of 0 Pa was set for pressure.

- Walls:

At tundish walls, including dams and weirs, no-slip conditions were prescribed. An automatic near wall treatment was applied for SST model and a scalable wall function for $k-\varepsilon$ model (Ansys CFX, 2011). For the non-isothermal analysis, a prescribed flux of 9000 W/m^2 was set for all tundish walls, except for dams and weirs, which were considered to be adiabatic (De Kock, 2005). When considering Lagrangian analysis, a restitution coefficient equal to 1 was applied; Therefore, all collisions were considered to be perfectly elastic.

- Free surface of steel bath:

At the slag cover, free-slip condition (zero shear stress) was applied. Furthermore, a prescribed flux of 18000 W/m^2 was applied (De Kock, 2005). For Lagrangian analysis, a restitution coefficient equal to 0 was applied; Therefore, all particles that collided with the slag layer were captured.

- Symmetry plane:

In order to take advantage of symmetry of the investigated tundishes, only half tundish configuration was used and hence, at symmetry plane, values of the normal velocity component as well as scalar variable gradients normal to the boundary, were set to zero.

The flow field obtained from the steady-state analysis was used for solving both the Lagrangian tracking equation and transient tracer convection-diffusion equation in order to obtain the quantity of particles removed at slag layer and RTD curve, respectively. The initial and boundary conditions used for solving the tracer concentration are stated as follows:

- At $t = 0$:

As initial condition, values of 0 kg/m^3 for tracer concentration were applied.

- Boundary conditions:

Zero tracer gradient concentration for all tundish walls were employed. At the inlet region, a pulse tracer injection was prescribed (inlet concentration of 1 kg/m^3 during a time interval of 1s).

5 NUMERICAL MODELING

There are many software packages available for modeling and computing the physical phenomena that occur within the tundish, such as Fluent, CFX, Phoenics, Comsol, and so on. The present study employs the commercial software Ansys CFX. This software is based on Element-based Finite-Volume method (EbFVM) to discretize the partial differential equations arising from physical model. Moreover, it uses a coupled solver, thus mass and momentum equations are solved as a single system.

5.1 Physical and operating parameters for all cases

Three validation case studies were analyzed in the present work. Table 5.1 shows the physical and operating parameters for all validation case studies. Validation case I is an experimental work of Kemeny et al. (1981), validation case II is an experimental work of Wollmann (1999), and validation case III is a numerical work of Daoud (2006), which used the same geometry and operating parameters of the work of Wollmann (1999).

Table 5.1 – Physical and operating parameters for validation cases.

	Validation case I	**Validation cases II and III**
Volume - m³	4,39	1,8
Inlet diameter - m	0,051	0,065
Outlet diameter – m	0,076	0,036
Inlet mass flow rate – Kg/s	3,82	0,83

In addition, three new case studies were performed in the present wok. Tables 5.2 and 5.3 show the physical and operating parameters, respectively. Furthermore, it is worth to mention that all data set are based on actual continuous casting process of a local steelmaker company. Finally, actual physical and operating parameters are found in a specific range in order to control the continuous casting process; however, in the present work, mean values were adopted.

Table 5.2: Physical parameters for case studies.

Case I – Volume	0,663 m³
Case II – Volume	0,653 m³
Case III – Volume	0,631 m³
Inlet diameter	0,0215 m
Outlet diameter	0,0125 m
Weir height	0,35 m
Dam height	0,20 m

Table 5.3: Operating parameters for case studies.

Casting speed	2,7 m/min
Square cross section	120 mm
Inlet velocity	3,57 m/s
Inlet temperature	1823 K

Source: Da Silva (2015).

Finally, the basic tundish operating parameters, for instance, inflow rate and bath depth, as well as flow modifiers such as dams and weirs, may influence RTD values, and therefore the efficiency of the removal of inclusions can be drastically decreased if the aforementioned flow modifiers and operating parameters are misused (Mazumdar and Guthrie, 1999).

5.2 Solution procedure

In ANSYS CFX, the mass and momentum equations are solved coupled for pressure and velocity components using the Element-based Finite-Volume Method (EbFVM). After obtain the above variables, the turbulence model and energy equation are solved using a segregated approach. After the velocity and pressure fields reach the steady-state regime and for the non-isothermal simulation, the energy equation also reaches the steady-state regime, the concentration equation as well as the inclusion trajectory equation are solved to obtain the tracer behavior into the tundish and the particle trajectory, respectively. A second order high resolution scheme was used to discretize the convective terms for all conservation equations.

Finally, a second order backward Euler scheme was applied for the transient terms in order to make use of large timesteps without compromise the accuracy of the analysis.

The algebraic system of linear equations obtained after discretization are solved by an algebraic multigrid methodology called the additive correction multigrid method (Ansys CFX, 2011).

Convergence was achieved when the RMS (Root Mean Square) residuals were equal or smaller than 10^{-5} for mass, momentum and turbulence equations and 10^{-6} for tracer convective-diffusion and energy equations. A CPU time of about 5 hours for the steady-state simulations and 15 hours for the transient ones, was required.

5.3 Assumptions

The main assumptions adopted for modeling the continuous casting tundish are stated as follows:

- The fluid flow into the tundish was treated as a 3D turbulent and incompressible fluid flow. Constant values of the physical properties for steel and water were used to model the molten steel into the tundish for both isothermal and non-isothermal cases. The AISI 1025 steel properties were used for the non-isothermal simulations. These values are shown in Tables 2.1 (section 2.2) and 5.4.

Table 5.4: AISI 1025 steel thermophysical properties.

Thermal Conductivity	29 W/m.K
Specific heat	600 J/kg.K
Density	7000 kg/m^3
Dynamic viscosity	0,0064 Pa.s
Thermal expansivity coefficient	1,107x10^{-4} K^{-1}

Source: Bejan, 1993; De Kock, 2005.

- The slag layer was assumed to be flat and had a constant bath height. Furthermore, secondary reaction in both slag layer-air and slag layer-molten steel interface, were neglected.

- The heat loss due to radiation and convection were incorporated in heat fluxes at slag layer as well as for the lateral and bottom walls of the tundish, whereas the dams and weirs were assumed to be adiabatic.
- The effects of collision, coalescence, and reoxidation of particles as well as sticking to the walls were not accounted for the Lagrangian analysis. In addition, spherical particles with a specified diameter and having a constant density of 4000 kg/m^3 were employed.
- The tracer was treated as a passive scalar, meaning that its path throughout the tundish has no influence on the flow field.

5.4 Independence tests for grid, time, and number of injected particles

Independence tests for grid, time, and number of particles injected at inlet were performed for each case study. By taking advantage of the geometry symmetry only half tundish was chosen for all simulation cases, except for the validation of case I, where a quarter of the geometry was used due to the presence of two symmetry planes.

First of all, considering the mesh study, refinement was employed next to walls, in the inlet and outlet regions (where more complex flow pattern is expected to occur); for the rest of the tundish configuration a coarser grid was used.

In addition, unstructured meshes (composed by tetrahedral and prism elements) were applied in order to match the geometry shape of the solution domain. Fig 5.5 shows an unstructured mesh for case I, where just half tundish was considered.

Figure 5.1 – Cross section of a mesh for case I.

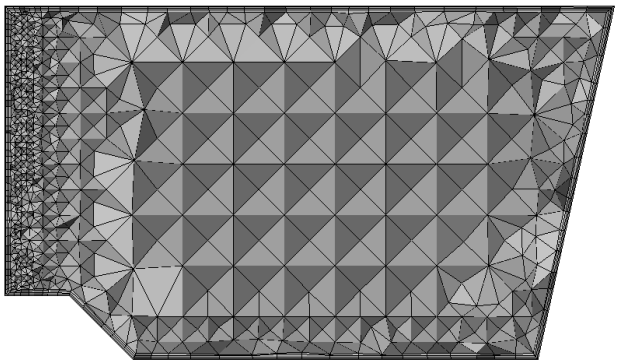

Finally, the following table summarizes the number of nodes used in all simulation cases. Also, appendix B brings a typical mesh study employed in the present work.

Table 5.5: Number of nodes used for each case study.

	Number of nodes
Validation Case I	98000
Validation Cases II and III	259000
Case I	64000
Case II	65000
Case III	66000

Secondly, regarding the time independence tests, one may not need to use small timesteps to guarantee numerical stability, since Ansys CFX is an implicit code. However, for some transient calculations (for example, the tracer concentration at the outlet tundish region), the timestep needs to be small in order to accurately obtain the time history of important parameters, such as the peak of concentration at the beginning of the simulation (Ansys CFX, 2006).

Therefore, after performing timestep studies for all case simulations, a timestep size of 1s was chosen for the first two validation cases, while a timestep size of 0.1s was chosen for the other three cases. Also, appendix C brings a typical timestep study employed in the present work.

Thirdly, an independence test was made to find out how many particles could describe the whole field of non-metallic inclusions injected at the inlet tundish region. For all Lagrangian case simulations a number of 1000 particles were found to be a good representation of the total number of particles. Appendix D brings a typical study for the number of particles injected at tundish inlet, which was employed in the present work.

6 RESULTS AND DISCUSSION

6.1 Validation cases

In order to obtain the numerical validation of the methodology employed in the present work, three validation cases were performed. Furthermore, for validation cases I and II, two turbulence models were tested, namely, the $k-\varepsilon$ model (Launder and Spalding, 1974) and SST model (Menter et al., 2003). (Geometries and meshes are shown at appendix A)

6.1.1 Validation case I

First, a validation case was performed by comparing the present work using two turbulence models with the experimental work of Kemeny et al. (1981). This validation was made by comparing the minimum and mean residence time from the present work and the experiments of the aforementioned work. The results can be seen in Table 6.1. As Daoud (2006) performed the same analysis, we also present the numerical results obtained by him in order to further enhance the validation.

Table 6.1 – Comparison with experimental and numerical analyses – Validation case I.

	θ_{min} [-]	θ_{mean} [-]
$k-\varepsilon$ model – Present work	0,097	0,959
SST model – Present work	0,104	0,951
Kemeny et al. (1981) - Physical modeling	0,070	0,800
Daoud (2006) - Numerical modeling	0,130	0,920

The obtained results from the present work, for both turbulence models, showed an acceptable agreement (from the engineering viewpoint) with both physical and numerical modeling from the literature. When comparing the efficiency between the two turbulence models, both of them showed similar results. While the $k-\varepsilon$ turbulence model presented closer values for the minimum residence time, the SST turbulence model pointed out a better approximation for the mean residence time. Therefore, since the difference between the two

turbulence models were minor, at least for this configuration, both of them can be used for representing the fluid flow into the given tundish.

6.1.2 Validation case II

The other validation case was performed by comparing the numerical results of this work using two turbulence models with the experimental work of Wollmann (1999). For this validation case study, we compare the RTD curves as well as the minimum and mean residence time from the present work with the experimental results of Wollmann (1999). The results are shown in Fig. 6.1.

Figure 6.1 – Comparison with experimental data for validation case II.
(a) Central exit nozzle (b) Lateral exit nozzle.

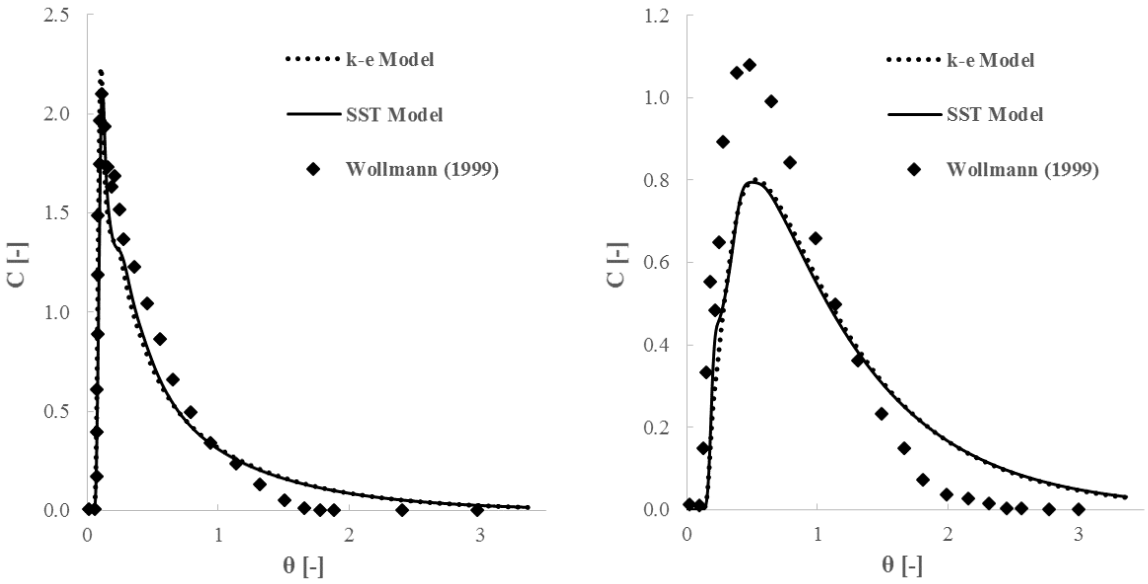

As it can be seen from Fig. 6.1, both turbulence models showed an acceptable agreement with the experimental work from the literature. Again, by comparing the accuracy between the two turbulence models, both of them showed similar results. However, if we carefully analyze the RTD curves for the central exit nozzle, the SST turbulence model showed better adjustment for the concentration peak. Therefore, for this T-delta-shaped tundish, the SST

turbulence model seems to be a better choice for characterizing the turbulence quantities. Finally, it is worthwhile to mention that despite of both turbulence models were able to predict the concentration peak of the RTD curves, they showed difficult to capture it properly in the RTD for the lateral exit nozzle. Therefore, further investigation needs to be performed in order to understand such behavior.

Table 6.2 compares the minimum and mean residence time extracted from the RTD curves showed above. The results from Daoud (2006) were also included in order to enhance the validation.

Table 6.2 – Comparison with experimental and numerical analyses – Validation Case II.

	θ_{min} [-]	θ_{mean} [-]
$k-\varepsilon$ Model – Present work	0,125	0,954
SST Model – Present work	0,129	0,954
Wollmann (1999) – Physical modeling	0,102	0,700
Daoud (2006) – Numerical modeling	0,165	0,910

Here, the results from the present numerical simulation, for both turbulence models, predicted both minimum and mean residence time with good accuracy when comparing with experimental and numerical study from the literature. Again, when comparing the efficiency between the two turbulence models, both of them showed similar results. Therefore, taking into account these two characteristic times, both turbulence models can be used for representing the fluid flow into the investigated tundish.

6.1.3 Validation case III

Even though the previous results for both turbulence models were only slightly different, we considered the drawbacks presented in section 2.7 regarding the $k-\varepsilon$ model; therefore, for validating the Lagrangian analysis only the SST turbulence model was used. For this validation case, the path of the particles, which simulate the non-metallic inclusions traveling into the tundish, is tracked. Two different cases were considered. The first one does

not take into account the turbulence dispersion; the second, on the other hand takes into account the use of the Random Walk Model (RWM) to simulate the chaotic effect of the turbulent eddies on the inclusion path. Fig. 6.2 does not consider the use of the RWM, whereas Fig. 6.3 presents the results by adding the RWM.

Figure 6.2 – Comparison with numerical data with no RWM.

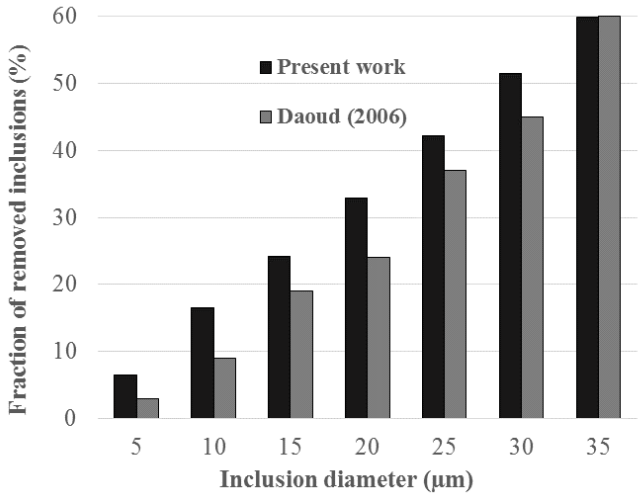

Figure 6.3 – Comparison with numerical data with RWM.

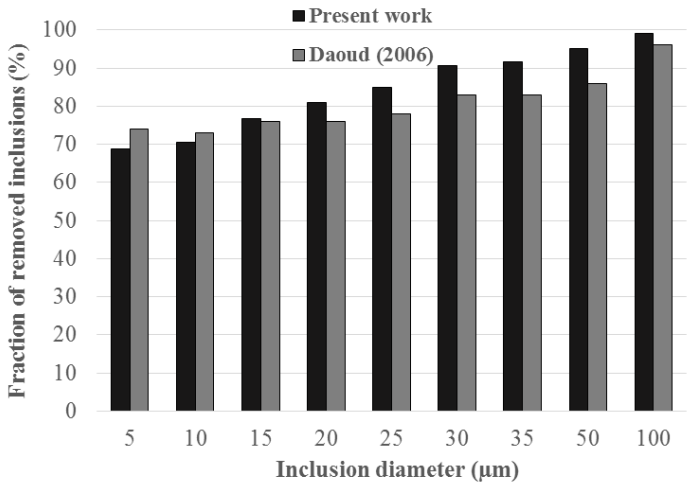

Both Figures 6.2 and 6.3 present the total amount of removed inclusion at the slag layer. From these figures, it is clear that when the RWM is used more inclusions can be removed. Finally, the numerical results showed, for most of diameter of the inclusions investigated, an acceptable agreement for both cases.

Considering that the results presented an acceptable agreement with both experimental and numerical analysis for all validation cases, and that the discrepancy between the comparisons can be attributed to some assumptions and the inherently deviation of the numerical studies from experimental ones, the methodology can be employed for the analysis of the actual tundish of a local steelmaker company. In addition, as both turbulence models presented similar results when the methodology was validated, we chose the SST turbulence model for the other numerical simulations.

6.2 Case studies for isothermal analysis

After validating the numerical methodology, the continuous casting tundish employed at a local steelmaker company was studied (Case I – Bare tundish). Furthermore, two more cases were performed in order to try to ameliorate the steel quality (Case II – Tundish with dam and Case III – Tundish with dam and weir). Once more, even though the previous results for both turbulence models were slightly different, we considered the drawbacks presented in section 2.7 regarding the $k-\varepsilon$ turbulence model, therefore, for all following case studies only the SST turbulence model was used.

In addition, the aforementioned considerations that were used in section 6.1 will be also applied in sections (6.2) and (6.3), which perform the isothermal and the non-isothermal analysis, respectively.

6.2.1 Flow field for the three case studies

Figs. 6.4 through 6.6 show the predicted velocity fields at different planes for the three case studies. For the sake of visualization, the figures depicting the inlet and outlet longitudinal planes show only half of the tundish.

When we consider the actual tundish configuration (case study I), we can see in Fig 6.4, at the inlet longitudinal plane, that a high turbulent jet from the inlet reaches the bottom of the tundish and spreads towards the outlet region. Once there is no baffle for this case, this spreading goes directly to the outlet region, which will probably cause the appearance of short-circuiting flow and the presence of inclusions at outlet nozzles.

Figure 6.4 – Isothermal flow pattern for case study I. (a) At the inlet longitudinal plane. (b) At the outlet longitudinal plane. (c) At the inlet transverse symmetry plane.

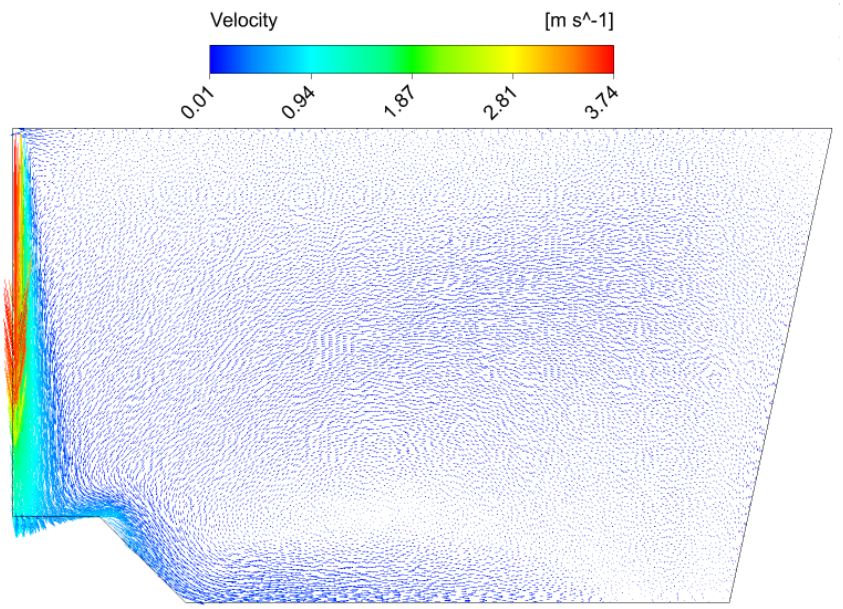

(a)

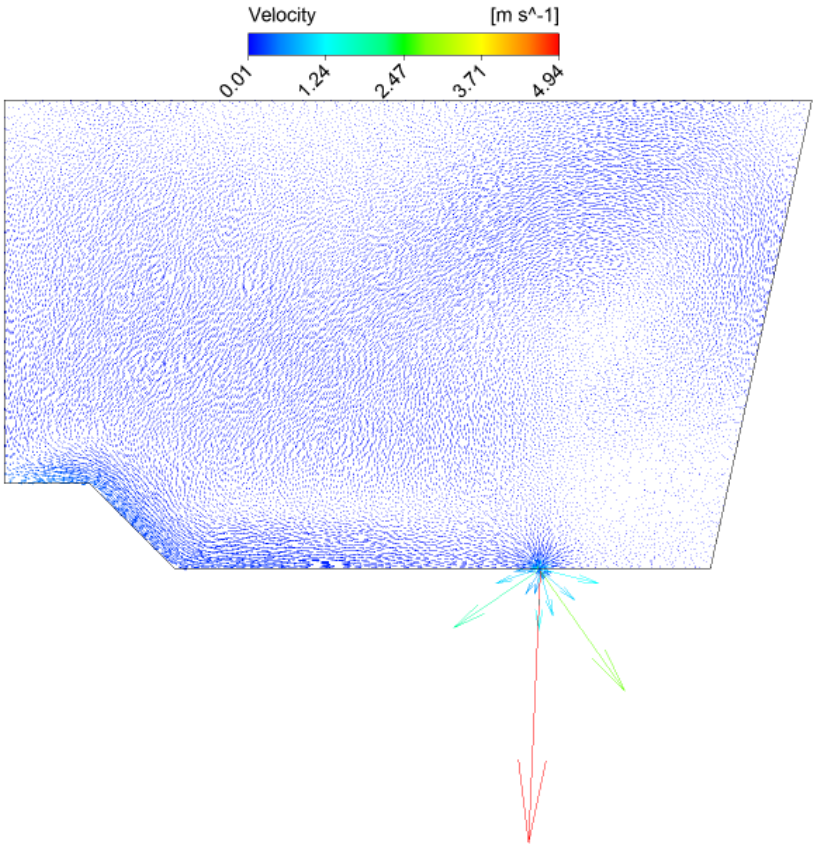

(b)

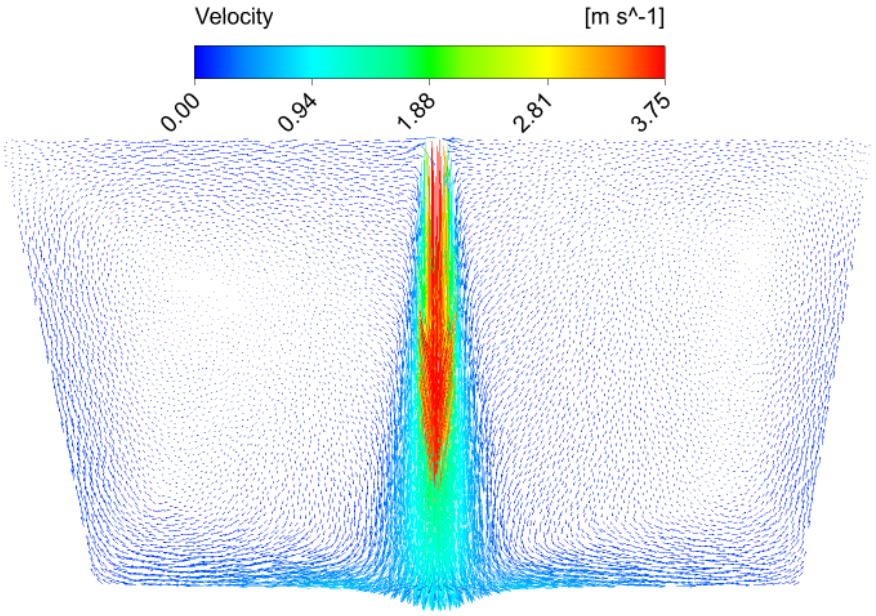

(c)

From Fig. 6.5, when we add dams to the actual tundish (case study II), the turbulence is confined at inlet regions, and the flow modifiers do not allow the incoming fluid to go directly to the outlet region. Moreover, by adding dams, recirculating zones appear in the same region, and this fact may improve the mixing extent, which may also lead to a better homogeneous mixture to the final product. However, these recirculating zones may also cause the decreasing in mean residence time and dispersed plug flow volume.

Figure 6.5 – Isothermal flow pattern for case study II. (a) At the inlet longitudinal plane. (b) At the outlet longitudinal plane. (c) At the inlet transverse symmetry plane.

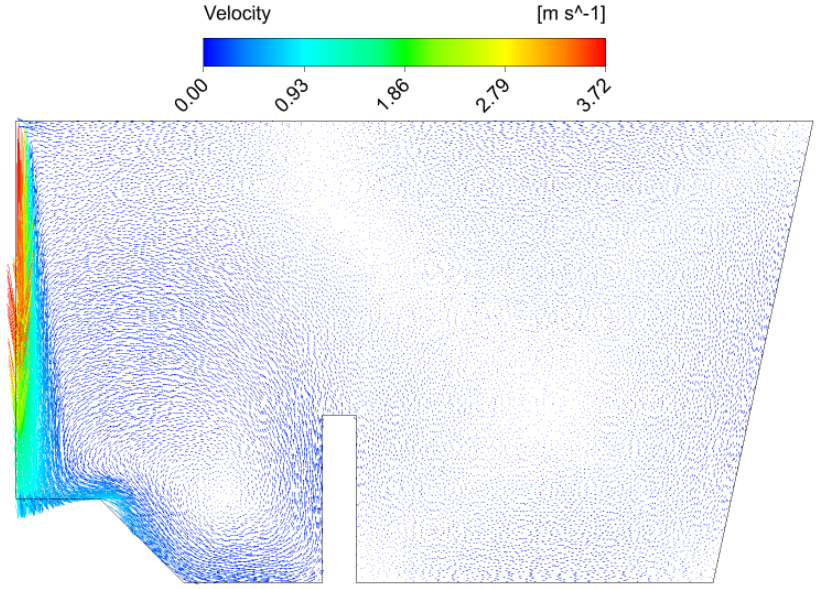

(a)

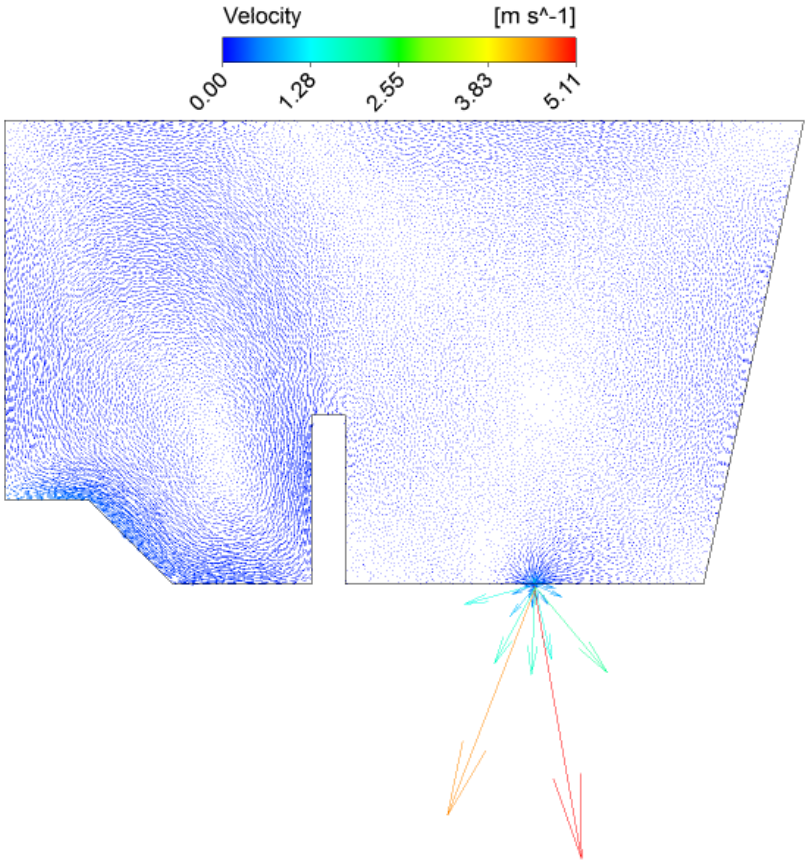

(b)

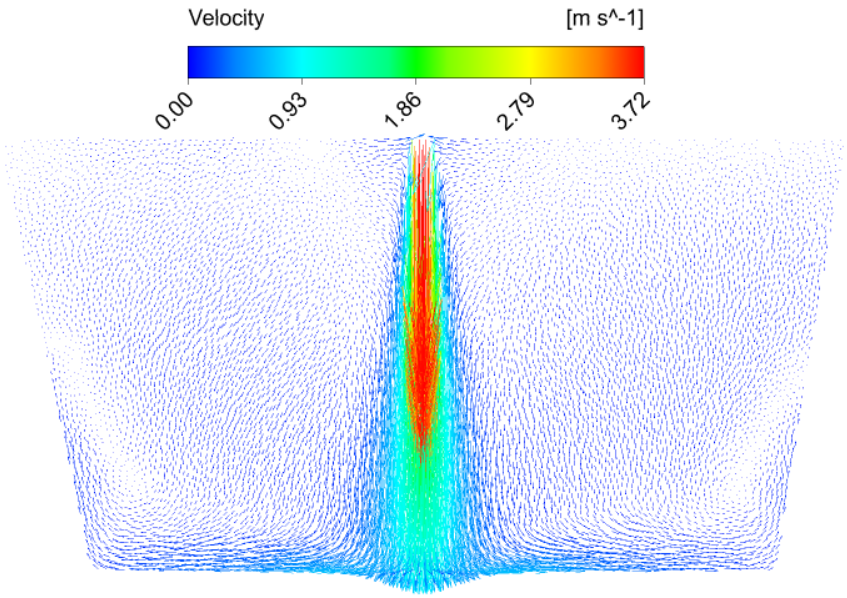

(c)

When weirs are added along with dams (case study III), similar conclusions verified to the case with only dams are observed (see for instance, Fig. 6.5). In addition, as one can see in Fig. 6.6 (c) higher values of mixing extent may appear, owing to the presence of high velocity values at the inlet transverse symmetry plane.

Figure 6.6 – Isothermal flow pattern for case study III. (a) At the inlet longitudinal plane. (b) At the outlet longitudinal plane. (c) At the inlet transverse symmetry plane.

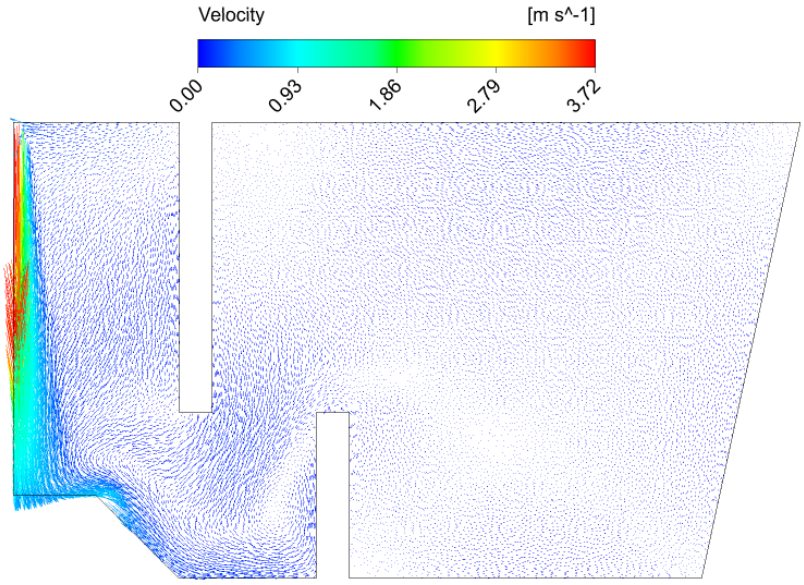

(a)

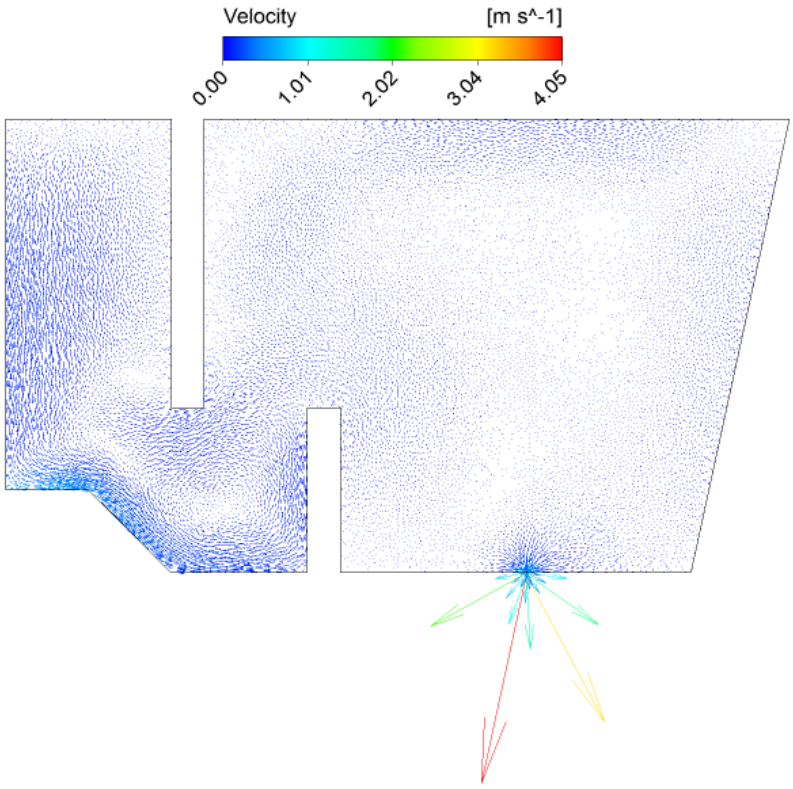

(b)

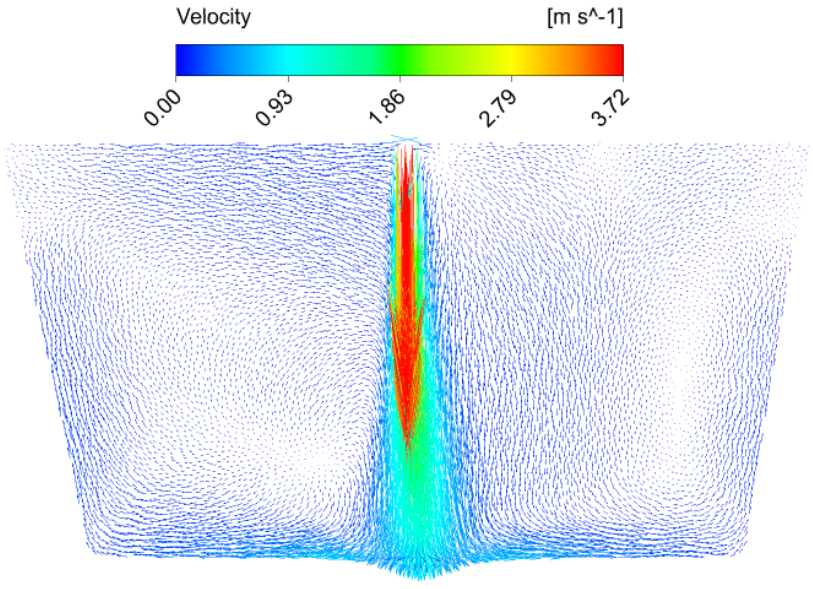

(c)

Finally, by comparing the magnitude of the velocity vectors at the outlet region, one can conclude that the insertion of flow modifiers decreased these values, which allows the flow to be more quiescent and does not carry inclusions for the following stages of the process.

6.2.2 RTD parameters for the three case studies

Fig. 6.7 shows the three case studies investigated, where they are confronted with each other in order to obtain a better configuration for improving the steel quality. This may be achieved by offering high values for both minimum and mean residence time.

For case I, a higher initial concentration peak is observed. This characterize the existence of short-circuiting volume, which promotes the carrying of non-metallic inclusions towards the exit nozzles, and then affecting the final steel quality. Also, this concentration peak appears early, which may carry inclusions from the inlet nozzle directly to the outlet nozzles.

In addition, it is observed that once flow control modifiers were introduced, this undesirable volume drastically decreased, in fact with the addition of weirs, this undesirable volume is almost vanished. Also, the absence of short-circuiting can be visualized as the C-curves present a significant displacement when the three cases are compared, indicating that the first fluid elements are spending more time into the vessel until they exit the tundish, which promotes an increase in the minimum and mean residence time.

Figure 6.7 – Comparison of the three cases – Isothermal analysis. (a) RTD curves for the whole simulation time. (b) RTD curves showing the concentration peaks.

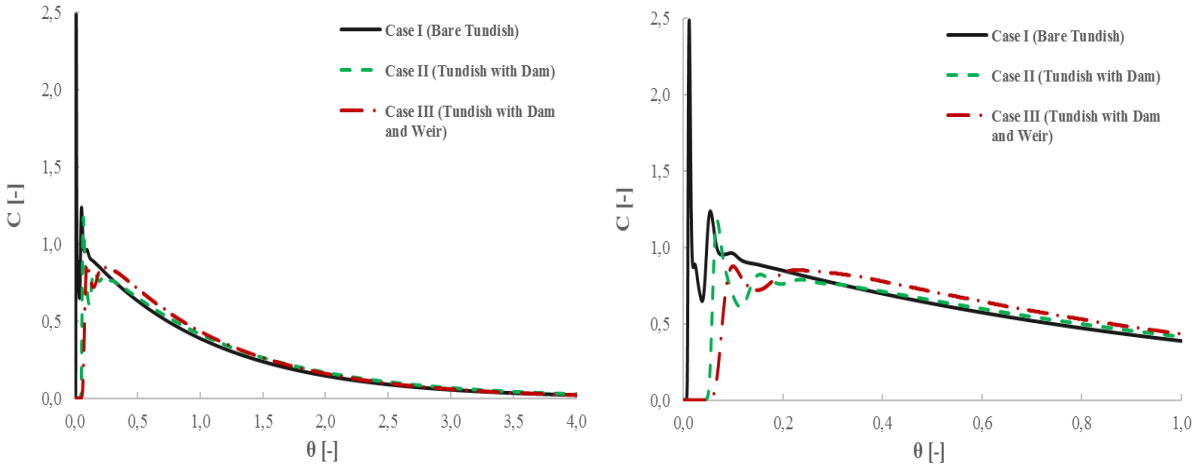

(a) (b)

Table 6.3 corroborates the previous observed results. From this table, we can see an increase in both minimum and mean residence time for fluid elements into the tundish as flow modifiers are added, which is very important for steel cleanliness once inclusions have more time to float out, and consequently the inclusions can be captured by the slag layer.

Table 6.3: Minimum and mean residence time for each configuration – Isothermal analysis.

	θ_{min} [-]	θ_{mean} [-]
Case I	0,0078	0,989
Case II	0,051	1,12
Case III	0,062	1,08

Furthermore, in order to improve the steel quality, dead volume needs to be minimized, dispersed plug volume maximized, and well-mixed volume be kept in a suitable value (Sahai and Ahuja, 1986). Table 6.4 shows that these requirements have been achieved as long as one makes use of flow modifiers. As expected, a better performance was achieved for the case study III, where the combination of dams and weirs showed the best efficiency. Hence, the use of flow control devices has been justified.

Table 6.4: Volume fraction of flow – Isothermal analysis.

	Dead Volume (%)	**Dispersed plug Volume (%)**	**Well Mixed Volume (%)**
Case I	37,30	0,99	61,71
Case II	32,96	5,94	61,10
Case III	30,98	8,12	60,90

6.2.3 Lagrangian analysis for the three case studies

According to Miki and Thomas (1999), the use of the Random Walk Model (RWM) to simulate the chaotic turbulent effects is considered to be more representative of the turbulent state in an actual tundish. As a result, all of the remainder simulations were performed by taking into account the use of the RWM. Fig. 6.8 shows the fraction of captured inclusions at the slag cover as function of a range of particle diameters.

Figure 6.8 – Lagrangian analysis for the three cases with RWM – Isothermal analysis.

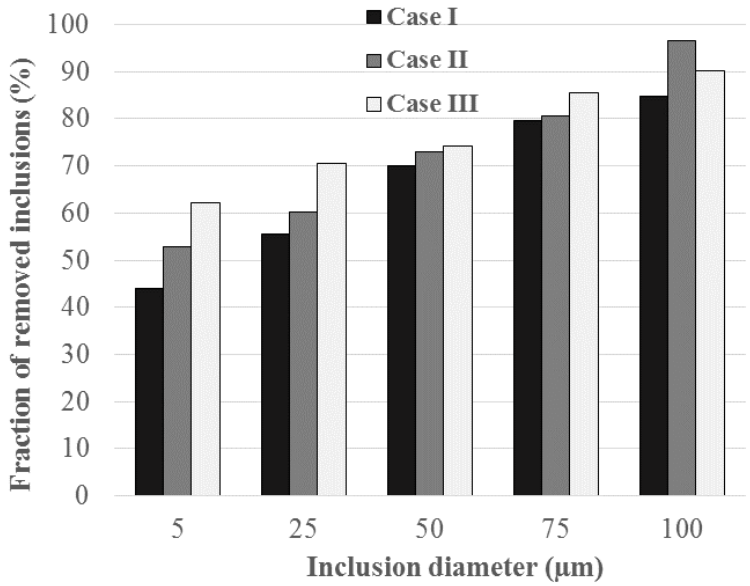

From Fig. 6.8, it is clear that the larger the diameter of the inclusions, the greater is the efficiency of the inclusions removed. This was already expected since inclusions with large diameters tend to be more susceptible to float out and to be captured by the slag layer through buoyancy force mechanism. Also, for the whole range of inclusion diameter, the addition of flow control devices enhances the inclusion removal at the slag layer. The combination of dams and weirs shows better efficiency with all particle diameter, except with the largest particles, where the configuration with just dams had a better performance.

6.3 Case studies for non-isothermal analysis

As mentioned before, for all case studies the SST turbulence model was used.

6.3.1 Temperature field for the three case studies

Figs. 6.9 throught 6.11 depict the temperature distribution in specified planes of the investigated tundishes. From Fig. 6.9, considering the case study I, it can be seen that the hottest molten steel is concentrated at the inlet region, while the bulk fluid region presents regions of lower liquid steel temperature. This can be considered a favorable situation to promote fluid

homogenization. Furthermore, the coolest liquid steel occurs at the corner of the tundishes, where dead regions are also present. This is an undesirable situation, since the more the molten steel stays in these regions, the more is the chance to the liquid steel solidify into the tundish and not be carried to the molds.

From Fig 6.9 (c), which is localized at the inlet tranverse symmetry plane, it is noticed that there is no symmetry in temperature contours since the actual tundish does not have longitudinal symmetry.

Figure 6.9 – Temperature contours for case study I. (a) At the inlet longitudinal plane. (b) At the outlet longitudinal plane. (c) At the inlet transverse symmetry plane.

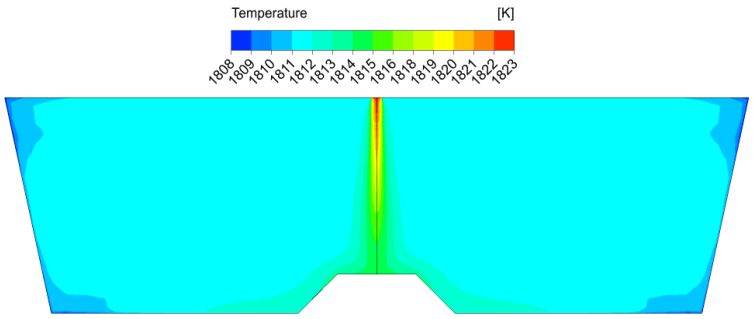

(a)

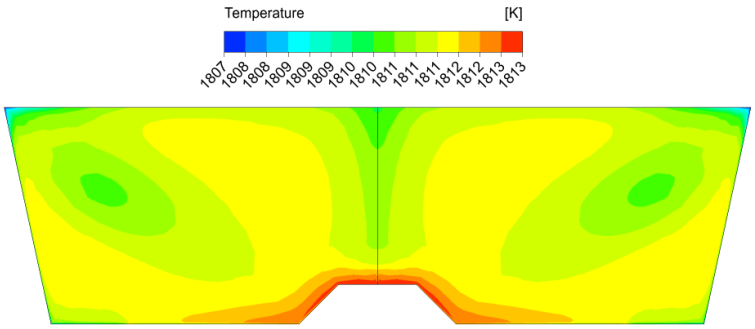

(b)

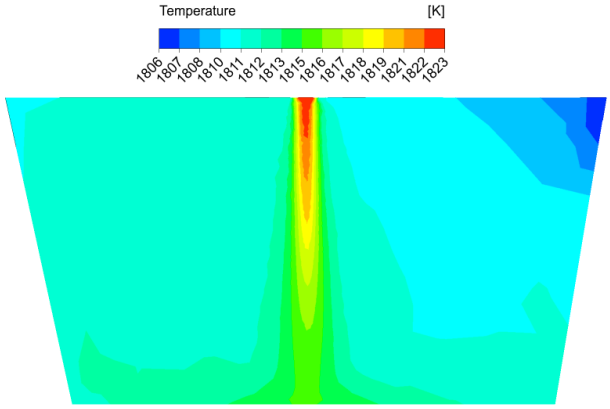

(c)

Fig. 6.10 shows the temperature profiles at different planes for the case study II. From that figure it is noticeable that by inserting dams, the hottest molten steel is concentrated in a larger region than it was for the case study I. This situation favors the mixing of the inlet hot jet provided by the ladle and the existing fluid into the tundish. However, by adding dams it is created cooler regions behind them, and also cooller regions are increased at the inlet of the tranversal symmetry plane.

Figure 6.10 – Temperature contours for case study II. (a) At the inlet longitudinal plane. (b) At the outlet longitudinal plane. (c) At the inlet transverse symmetry plane.

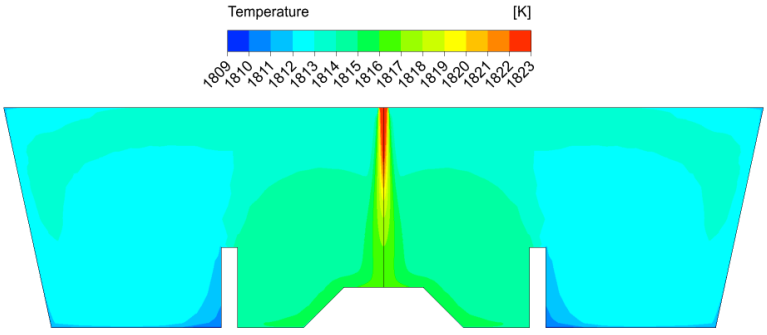

(a)

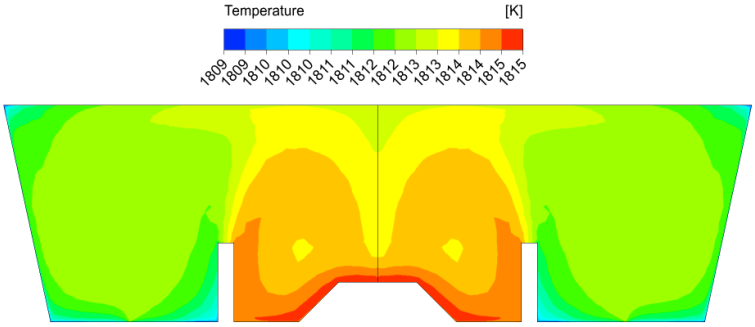

(b)

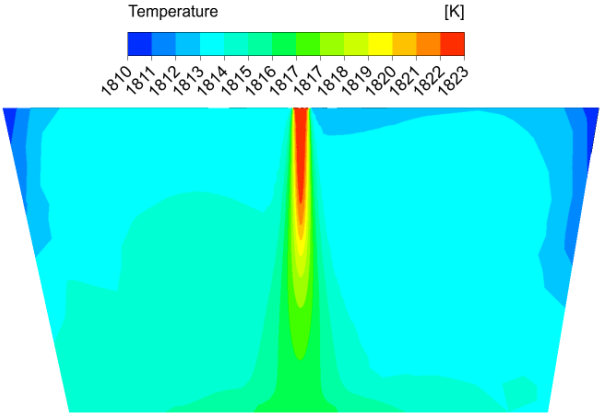

(c)

Fig. 6.11 presents the temperature field for the case study III. From this figure, it can be seen that by inserting weirs, the inlet region increases the concetration of the hottest molten steel. In addition, cooller regions presented at corners and behind dams seem to be reduced significantly.

Figure 6.11 – Temperature contours for case study III. (a) At the inlet longitudinal plane. (b) At the outlet longitudinal plane. (c) At the inlet transverse symmetry plane.

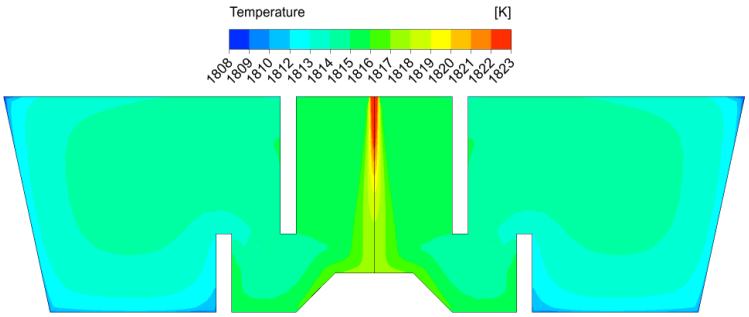

(a)

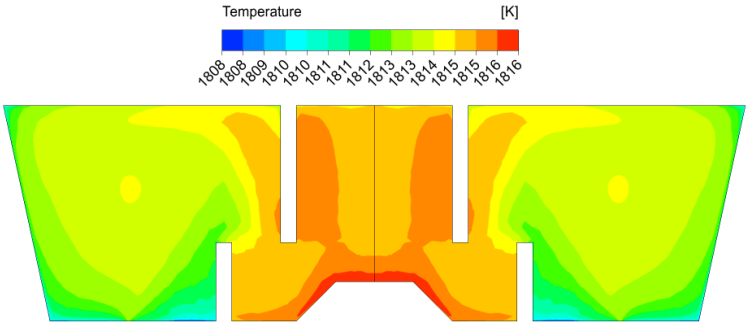

(b)

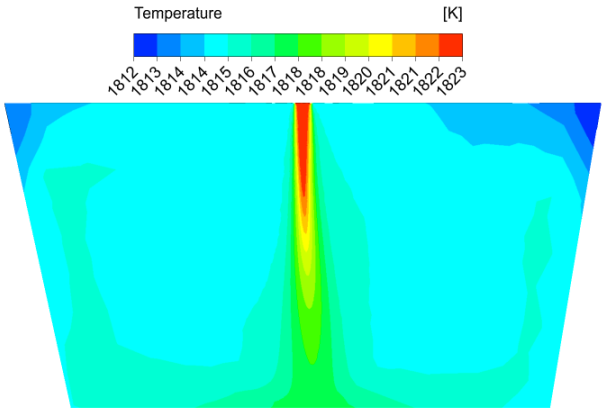

(c)

6.3.2 RTD parameters for the three case studies

The RTD curves for all non-isothermal cases as wells as the characteristic times and volumes are presented in Fig. 6.12, Table 6.5, and Table 6.6, respectively. As we can see from these results, there is no significant difference between the results achieved with isothermal analysis and non-isothermal one. Therefore, similar considerations can be drawn for both analysis, and for the sake of simplicity, they will not be repeated here. Also, the results obtained in the present work did not present expected differences when comparing some aspects of both isothermal and non-isothemal simulations, for instance, different RTD curves (see the work of Alizadeh et al. (2008)). However, this fact may be attributed to the fact that the tundish volume employed by Alizadeh et al. (2008) was about twice larger than the tundish employed in the present work.

Figure 6.12 – Comparison of the three cases – Non-isothermal analysis. (a) RTD curves for the whole simulation time. (b) RTD curves showing the concentration peaks.

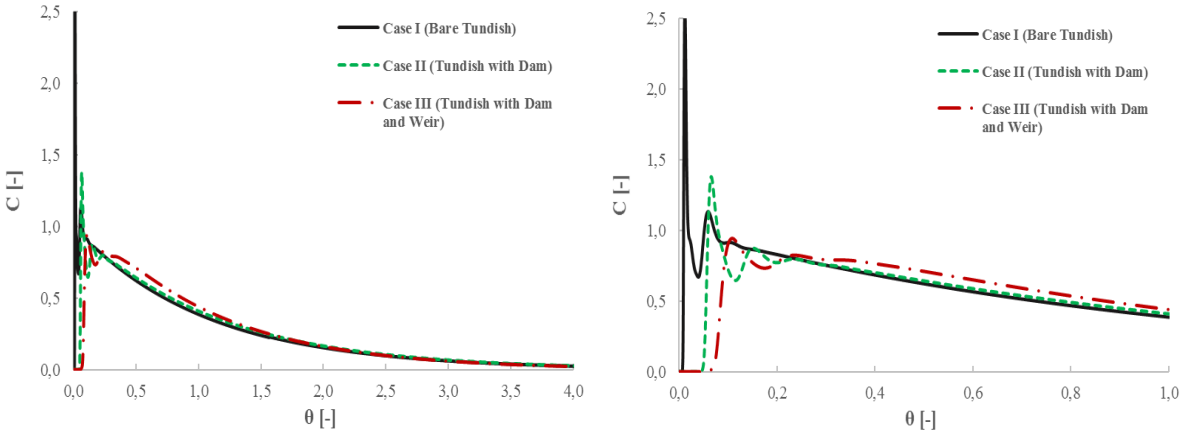

(a) (b)

Table 6.5: Minimum and mean residence time for each configuration – Non-isothermal analysis.

	θ_{min} [-]	θ_{mean} [-]
Case I	0,0076	1,029
Case II	0,05	1,115
Case III	0,07	1,092

Table 6.6: Volume fraction of flow – Non-isothermal analysis.

	Dead Volume (%)	**Dispersed plug Volume (%)**	**Well Mixed Volume (%)**
Case I	37,03	1,03	61,94
Case II	33,65	5,80	60,55
Case III	30,47	9,07	60,46

6.3.3 Lagrangian analysis for the three case studies

Fig. 6.13 shows the fraction of removed inclusions at the slag layer for non-isothermal case. Unlike the Eulerian analysis for isothermal and non-isothermal case, the Lagragian analysis showed different results when comparing the quantity of particles removed at slag layer. As expected, the presence of buoyancy forces increased the removal of non-metallic inclusions. Also, considering small particles, the case study III appears to be the best configuration to adopt, whereas for large particles, namely, particles with diameters of 75 μm and 100 μm , the case study II presented better efficiency of removal. The results showed here are in accordance with the work of Miki and Thomas (1999).

Figure 6.13 – Lagrangian analysis for the three cases with RWM – Non-isothermal analysis.

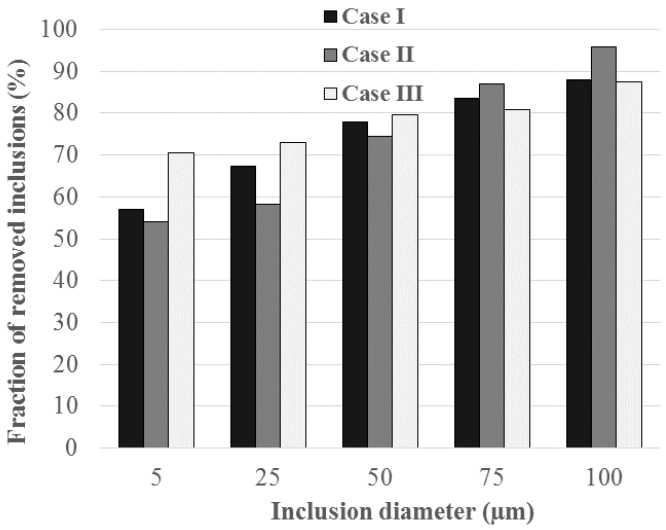

7 CONCLUSION AND FUTURE WORK

In the present work, a methodology has been developed to give a better configuration in order to enhance the steel cleanliness in an actual steel continuous casting tundish. This methodology makes use of the Computational Fluid Dynamics (CFD) techniques and employed the commercial software Ansys CFX, which uses the Element-based Finite-Volume Method (EbFVM) to discretize the partial differential equations arising from the physical model.

The methodology was validated using two experimental studies for Eulerian analysis and one numerical study for Lagrangian analysis. Also, the methodology showed good agreements with the works from the literature. From this analysis, it is concluded that the methodology can be applied for the case studies of interest. The first case study was an actual tundish configuration (case I – Bare tundish), and two more cases with some geometric modifications were proposed to the original configuration, namely, case II – Tundish with dam, and case III – Tundish with dam and weir.

One drawback which appears in the present work was the fact that the isothermal and non-isothermal Eulerian analysis did not show significant difference in RTD curves and characteristic times and volumes. However, this should not take the merits of this methodology away since this fact may be attributed to the fact that the tundish volume employed by Alizadeh et al. (2008), in which work there were difference between the aforementioned analysis, was about twice larger than the tundish employed in the present work.

As observed, as soon as flow control devices were inserted into the actual tundish, the minimum and mean residence time were increased. In addition, the characteristic volumes satisfied the required criteria to increase the steel quality. Furthermore, considering the Lagrangian analysis, the fraction of removed inclusions at the slag cover increased by making use of these flow modifiers.

Therefore, the use of such flow control devices provides an efficient and reliable way to promote inclusion flotation towards the slag layer in order to capture and remove them, and consequently promotes the enhancement of steel cleanliness.

Finally, by confronting all case studies, it is concluded that by simply adding dams the steel quality can be already enhanced and for some specific cases this simply addition showed better results than the case with dams in conjunction with weirs. Nevertheless, for overall cases, the best configuration to be used is the one with dam and weir (case III).

7.1 Future work

In order to perform a more detailed study it is recommended the following analysis for future researches:

- Perform an experimental work in order to analyze the fluid flow and heat transfer for both the actual tundish configuration and the proposed modifications through the use of flow modifiers;
- Combine CFD techniques with mathematical optimizers to achieve the best position into the given tundish for all flow control devices;
- Test different models of turbulence. The Ansys CFX itself has most of the available models, such as the $k-\omega$ model, the RNG (Re-Normalization Group $)k-\varepsilon$ model, the RSM (Reynolds Stress models) turbulence models, and so on;
- Carry out transient analysis for solving the fluid flow and heat transfer into the tundish, since the actual operations in the continuous casting process involve transient periods.

REFERENCES

ALIZADEH, M.; EDRIS, H.; SHAFYEI, A., Fluid flow and mixing in non-isothermal water model of continuous casting tundish, **Journal of Iron and Steel Research, International**, v. 15, p. 07-13, 2008.

ALVES, J. G., **Improvement in the pattern of liquid steel flow in the APERAM stainless South America continuous casting tundish 01**, Thesis. Graduate Program in metallurgical, materials and mining engineering. Federal University of Minas Gerais, Belo Horizonte, 2014. (In Portuguese)

ARGYROPOULOS, C.D.; MARKATOS, N.C., Recent advances on the numerical modelling of turbulent flows, **Applied Mathematical Modelling**, v. 39, p. 693-732, 2015.

BEJAN, A., **Heat transfer**. New York, John Wiley & Sons, 1993.

BENSOUICI, M.; BELLAOUAR, A.; TALBI, K., Numerical investigation of the fluid flow in continuous casting tundish using analysis of RTD curves, **Journal of Iron and Steel Research, International**, v. 16, p. 22-29, 2009.

CHAKRABORTY, S.; SAHAI, Y., Mathematical modelling of transport phenomena in continuous casting tundishes. Part 1 – transient effects during ladle transfer operations, **Ironmaking and steelmaking**, v. 19, p. 479-487, 1992.

CHATTOPADHYAY, K.; ISAC, M.; GUTHRIE, R. I. L, Physical and mathematical modelling of steelmaking tundish operations: A review of the last decade (1999-2009), **ISIJ International**, v. 50, p. 331-348, 2010.

CROWE, C.; SOMMERFELD, M.; TSUJI, Y., **Multiphase flows with droplets and particles**, CRC Press, New York, London, 1998.

DAOUD, I. L. A., **Numerical study of the flow and behavior of non-metallic inclusions in steel continuous casting tundishes**, Thesis. Graduate Program in mining, metallurgical and materials engineering. Federal University of Rio Grande do Sul, Porto Alegre, 2006. (In Portuguese)

DA SILVA, F. D. A., **Quality optimization on continuous casting of billets through the use of mathematical models**, Thesis. Graduate Program in Mechanical engineering. Federal University of Pernambuco, Recife, 2015. (In Portuguese)

DE KOCK, D.J., **Optimal tundish design methodology in a continuous casting process**, Philosophiae Doctor, University of Pretoria, Pretoria, 2005.

FERNANDES, B. R. B., **Implicit and semi-implicit techniques for the compositional petroleum reservoir simulation based on volume balance**, thesis. Graduate Program in Chemical Engineering. Federal University of Ceará, Fortaleza, 2014.

FILIPPINI, G.; MALISKA, C. R.; VAZ Jr., M., A physical perspective of the element-based finite volume method and FEM-Galerkin methods within the framework of the space of finite elements, **International Journal for Numerical Methods in Engineering**, v. 98, p. 24-43, 2014.

GARDIN, P.; BRUNET, M.; DOMGIN, J.F.; PERICLEOUS, K., An experimental and numerical CFD study of turbulence in a tundish container, **Applied Mathematical Modelling**, v. 26, p. 323-336, 2002.

ILEGBUSI, O. J., Application of the two-fluid model of turbulence to tundish problems, **ISIJ International**, v. 34, p. 732-738, 1994.

INCROPERA, F. P.; DEWITT, D. P., **Fundamentals of heat and Mass Transfer**, 3rd edition, Wiley, New York, 1990.

ISHII, T.; KUBO, N.; BOSE, T. K.; IGUCHI, M., Mathematical modeling of flow and inclusion motion in vessel with natural convection, **ISIJ International**, v. 41, p. 1174-1180, 2001.

JAVUREK, M., CFD-modeling of inclusion behavior during ladle exchange in a continuous casting system, 5th World Congress on Computational Mechanics, Vienna, Austria, 2002.

JHA, P.K.; DASH, S.K., Employment of different turbulence models to the design of optimum steel flows in a tundish, **International Journal of Numerical Methods for Heat and Fluid flow**, v. 14, p. 953-979, 2004.

JOO, S.; HAN, J. W.; GUTHRIE, R. I. L, Inclusion behavior and heat transfer phenomena in steelmaking tundish operations: Parte II. Mathematical model for liquid steel in tundishes, **Metallurgical transaction B**, v. 24, p. 767-777, 1993.

JUN, W.; MIAO-YONG, Z.; HAI-BING Z.; YING, W.; Fluid flow and interfacial phenomenon of slag and metal in continuous casting tundish with argon blowing, **Journal of Iron and Steel Research, International**, v. 15, 26-31, 2008.

KEMENY, F.; HARRIS, D. J.; MCLEAN, A.; MEADOWCROFT, T. R.; YOUNG, J. D.; Fluid flow studies in the tundish of a slab caster, Process Technology Conference, v. 2, p. 232-245, 1981.

KRUGER, M., **Development of a computational procedure to the study of flow inside continuous casting tundishes**, Thesis. Graduate Program in mechanical engineering. Federal University of Santa Catarina, Florianópolis, 2010. (In Portuguese)

KUMAR, A.; KORIA, S.C.; MAZUMDAR, D., An assessment of fluid flow modelling and residence time distribution phenomena in steelmaking tundish systems, **ISIJ International**, v. 44, p. 1334-1341, 2004.

LAUNDER, B.E.; SHARMA, B.I., Application of the energy dissipation model of turbulence to the calculation of flow near a spinning disk, **Heat Mass Transfer**, v. 1, p. 131-138, 1974.

LAUNDER, B. E.; SPALDING, D. B., The numerical computation of turbulent flows, **Computer Methods in Applied Mechanics and Engineering**, v. 3, p. 269-289, 1974.

LEVENSPIEL, O., **Chemical reaction engineering**, 3rd edition, Wiley & Sons Inc., New York, 1998.

MALISKA, C. R., **Heat transfer and computational fluid mechanics**, 2nd edition, LTC Editora, Rio de Janeiro, 2004. (In Portuguese)

MARCONDES, F.; SEPEHRNOORI, K., An element-based finite-volume method approach for heterogeneous and anisotropic compositional reservoir simulation, **Journal of Petroleum Science and Engineering**, v. 73, p. 99-106, 2010.

MAZUMDAR, D., Tundish metallurgy: towards increased productivity and clean steel, **Transactions of the Indian Institute of Metals**, v. 66, p. 597-610, 2013.

MAZUMDAR, D.; GUTHRIE, R.I.L., The physical and mathematical modelling of continuous casting tundish systems, **ISIJ International**, v. 39, p. 524-547, 1999.

MENDONÇA, A. F. G., **Assessment of the effect of gas injection over the inclusion flotation in a continuous casting tundish**, Thesis. Graduate Program in metallurgical, materials and mining engineering. Federal University of Minas Gerais, Belo Horizonte, 2016. (In Portuguese)

MENTER, F.; FERREIRA, J.C.; ESCH, T.; KONNO, B., The SST turbulence model with improved wall treatment for heat transfer predictions in gas turbines, Proceedings of the International Gas Turbine Congress, Tokyo, November, p. 2-7, 2003.

MIKI, Y.; THOMAS, B. G., Modeling of inclusion removal in a tundish, **Metallurgical and Materials transactions B**, v. 30B, p. 639-654, 1999.

OMRANIAN, S. A., **The computational of turbulent, buoyancy-driven flows in cavities**, Ph.M. thesis, University of Manchester, England, 2007.

PIMENTA, P. V. C. L., **Thermomechanical simulation of the continuous casting process using the element-based finite-volume method**, Thesis. Graduate Program in Engineering and materials Science. Federal University of Ceará, Fortaleza, 2014. (In Portuguese)

RAGHAVENDRA, K.; SARKAR, S.; AJMANI, S. K.; DENYS, M. B.; SINGH, M. K., Mathematical modelling of single and multi-strand tundish for inclusion analysis, **Applied Mathematical Modelling**, v. 37, p. 6284-6300, 2013.

RAY, S. K., **On the application of physical and mathematical modeling to predict tundish performance**, PhD thesis, McGill University, Canada, 2009.

SAHAI, Y.; AHUJA, R., Fluid flow and mixing of melt in steelmaking tundishes, **Ironmaking and Steelmaking**, v. 13, p. 241-247, 1986.

SAHAI, Y.; EMI, T., Melt flow characterization in continuous casting tundishes, **ISIJ International**, v. 36, p. 667-672, 1996.

SHADE, J.; SMITH, M. P.; PALMER, S. E., Doubling tundish volume at AK steel's Middletown works: Structural criteria, design consideration and operation results, **Ironmaking and Steelmaking**, v. 23, p. 93-103, 1996.

SZEKELY, J.; ILEGBUSI, O. J., **The physical and mathematical modeling of tundish operations**, Springer-Verlag, New York, 1989.

SINGH, S.; KORIA, S. C., Model Study of the dynamics of flow of steel melt in the tundish, **ISIJ International**, v. 33, p. 1228-1237, 1993.

SINGH, S.; KORIA, S. C., Study of fluid flow in tundishes due to different types of inlet streams, **Steel Research**, v. 66, 1995.

SHENG, D.Y.; JONSSON, L., Investigation of transient fluid flow and heat transfer in a continuous casting tundish by numerical analysis verified with non-isothermal water model experiments, **Metallurgical and Materials Transactions B**, v. 30, p. 979-985, 1999.

TIAN-PENG, Q.; CHENG-JUN, L.; MAO-FA, J., Numerical simulation for effect of inlet cooling rate on fluid flow and temperature distribution in tundish, **Journal of Iron and Steel Research, International**, v. 19, p. 12-19, 2012.

THOMAS, B. G., **Continuous casting of Steel**, Chapter 15 in Modeling for Casting and Solidification Processing, O. Yu, editor, Marcel Dekker, New York, p. 499-540, 2001a.

THOMAS, B. G., **Continuous casting**, The encyclopedia of materials: Science and Technology, K. H. J. Buschow, R. cahn, M. Flemings, B. Ilschner, E. J. Kramer, S. Mahajan, (D. Apelian, subject ed.) Elsevier Science Ltd., Oxford, Vol. 2, p. 1595-1599, 2001b.

User's guide for Ansys CFX Release 14.0, Ansys Inc., 2011.

VARGAS-ZAMORA, A.; MORALES, R. D.; DÍAZ-CRUZ, M.; PALAFOX-RAMOS, J.; DEMEDICES, L. G., Heat and mass transfer of a convective-stratified flow in a trough type tundish, **International Journal of Heat and Mass Transfer**, v. 46, p. 3029-3039, 2003.

VERSTEEG, H. K.; MALALASEKERA, W., **An introduction to computational fluid dynamics**, 2nd edition, Harlow, 2007.

YEH, J. L.; HWANG, W. S; CHOU, C. L., An improved fluid flow model for slab tundishes and its comparison with a full-scale water model, **Applied Mathematical modelling**, v. 18, p. 39-45, 1994.

YUAN, Q.; THOMAS, B. G., Transport and entrapment of particles in continuous casting of steel, 3rd International Congress on Science & Technology of steelmaking, Warrendale, EUA, p. 745-762, 2005.

WANG, G; YUN, M.; ZHANG, C.; XIAO, G.; Flow mechanism of molten steel in a single-strand slab caster tundish based on the residence time distribution curve and data, **ISIJ International**, v. 55, p. 984-992, 2015.

WILCOX, D. C., Reassessment of the scale-determining equation for advanced turbulence models, **AIAA J**., v. 26, p. 1299-1310, 1988.

WILCOX, D. C., **Turbulence modeling for CFD,** 3rd edition, Canada: DCW Industries, 2006.

WOLLMANN, A. M., **Flow studies in a continuous casting tundish**, Thesis. Graduate Program in mining, metallurgical and materials engineering. Federal University of Rio Grande do Sul, Porto Alegre, 1999. (In Portuguese)

WORLD STEEL ASSOCIATION, Steel Statistical Yearbook, **Economics committee**, Brussels, 2015.

ZHANG, L.; THOMAS, B. G., Inclusions in continuous casting of steel, XXIV National Steelmaking Symposium, Morelia, Mich, Mexico, November, 26-28, p. 138-183, 2003.

APPENDIX A

GEOMETRIES AND MESHES

This appendix shows all geometries and meshes for the validation cases as well as for the case studies, namely, Case I, Case II, and Case III. Validation cases were based on the works of Kemeny et al. (1981), Wollmann (1999), and Daoud (2006).

Figure A.1 – Geometry and surface mesh for Case I.

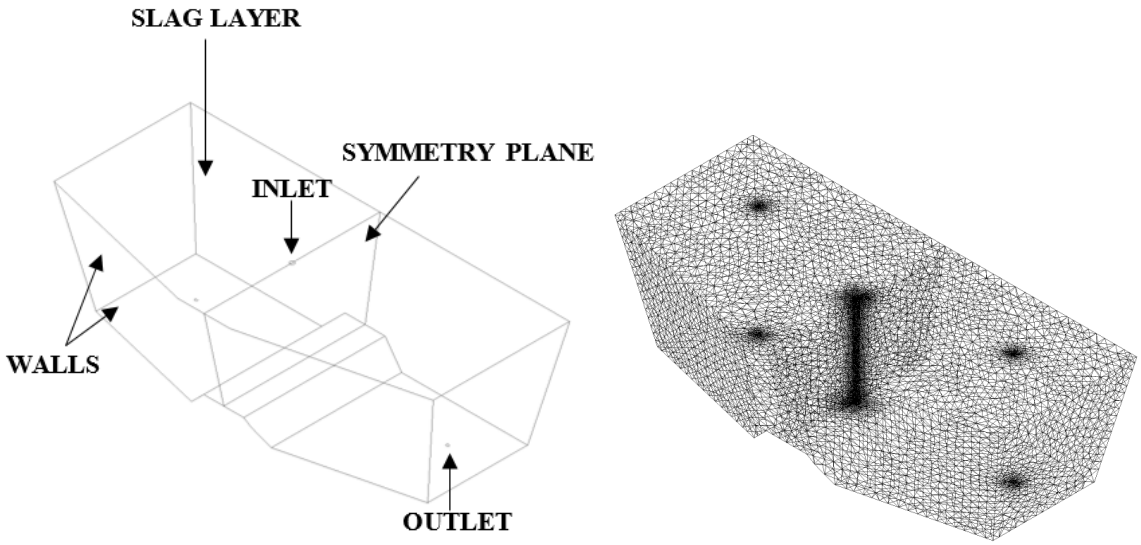

Figure A.2 – Geometry and surface mesh for Case II.

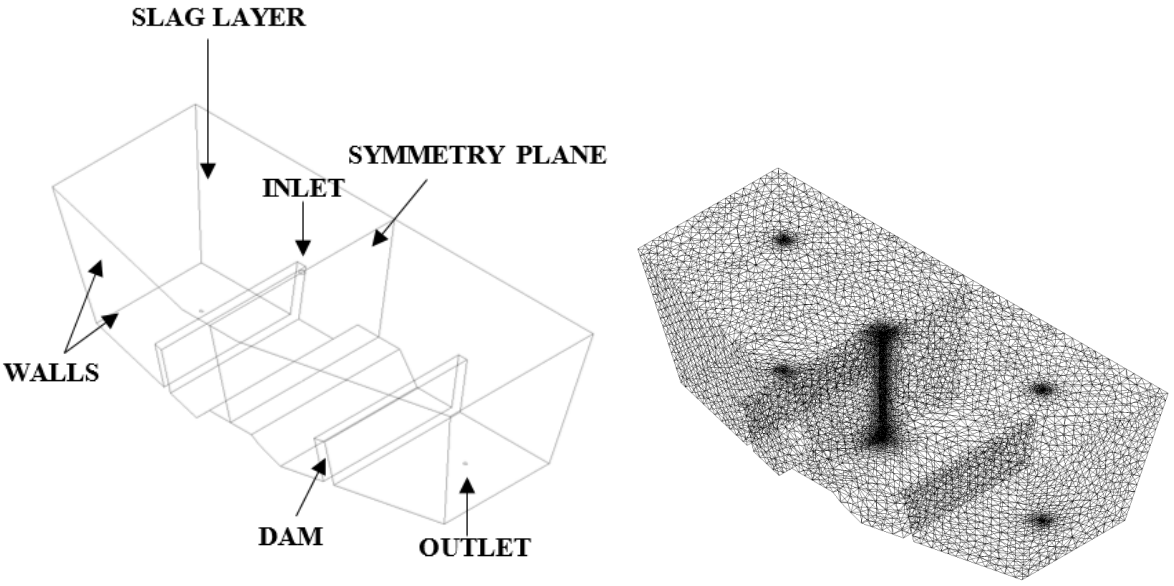

Figure A.3 – Geometry and surface mesh for Case III.

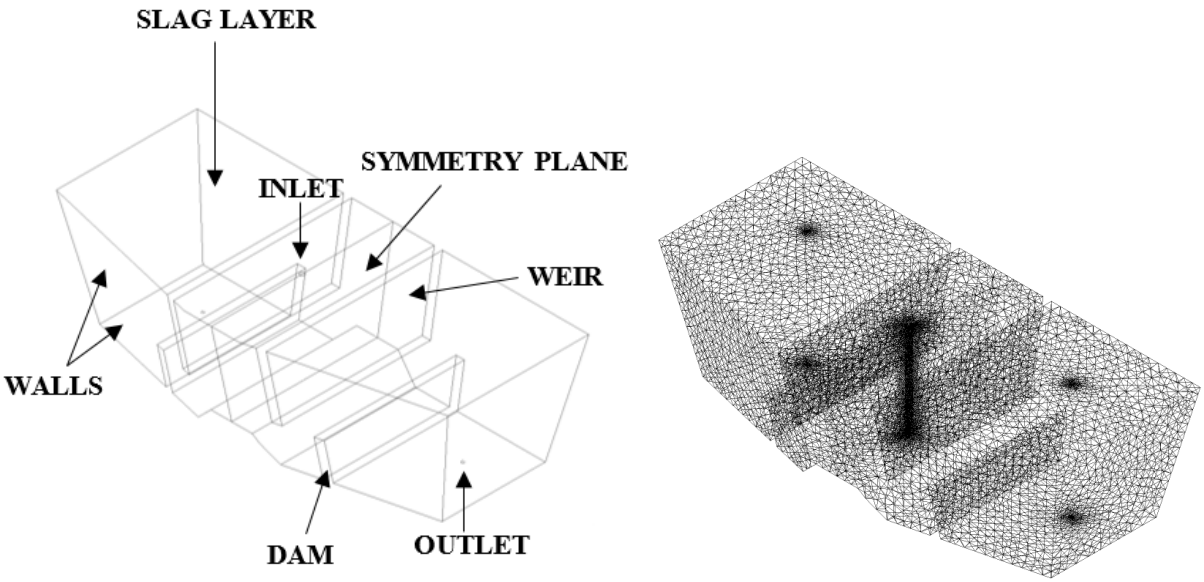

Figure A.4 – Geometry and surface mesh for the validation case I (Kemeny et al., 1981).

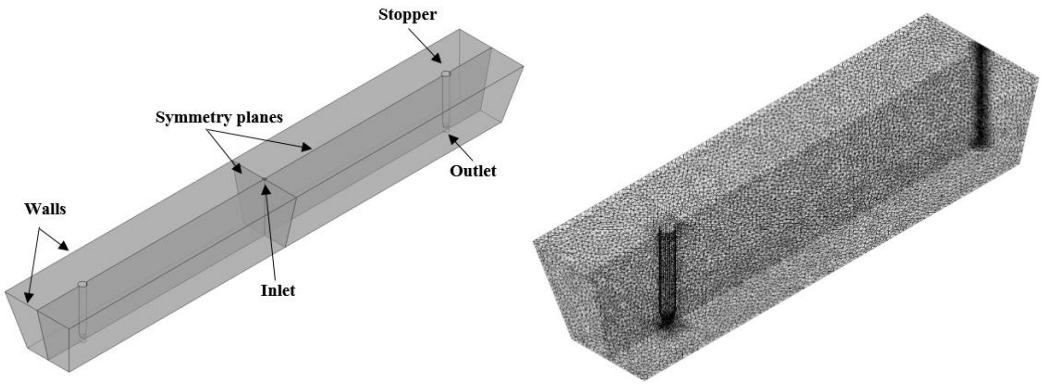

Source: Kemeny et al. (1981).

Figure A.5 – Geometry and surface mesh for the validation cases II and III (Wollmann 1999; Daoud, 2006).

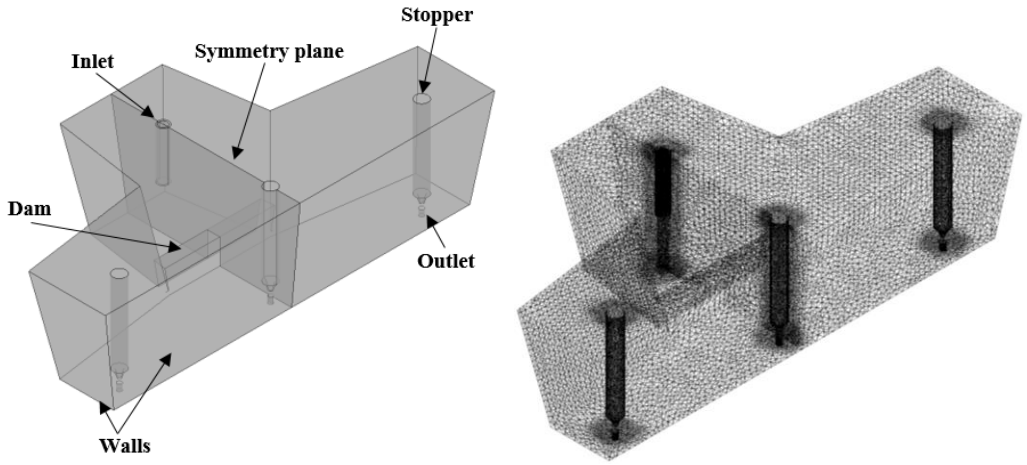

Source: Wollmann (1999).

APPENDIX B

MESH REFINEMENT STUDY

A mesh refinement study based on mean residence time, well-mixed volume, and dead volume was employed for all case studies. In this study, six types of non-uniform meshes composed by tetrahedral and prism elements were used, assuming a range of number of nodes varying from 4000 to 120000. In Fig. B.1, a mesh refinement study for case I using the SST model is shown.

Figure B.1 – Mesh refinement study for case I using SST model.

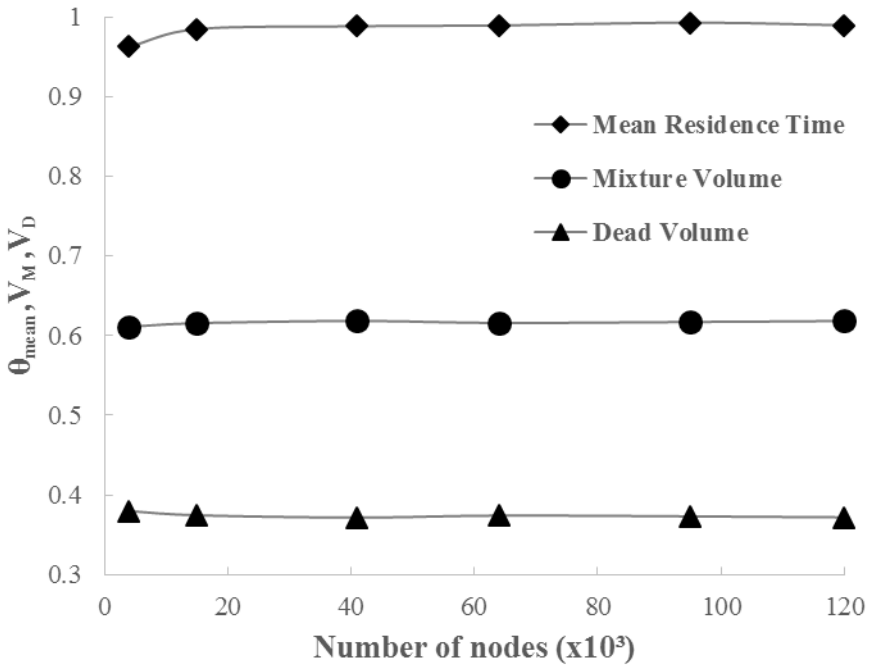

From the results presented above, it can be concluded that for meshes with more than 41000 nodes the mean residence, well-mixed volume, and dead volume do not present a significant variation; however, to be conservative, for case I, the mesh composed by 64000 nodes were used.

APPENDIX C

TIMESTEP CONVERGENCE STUDY

A study of timestep convergence on the RTD curves for all case studies was performed. Four different timesteps, ranging from 10 seconds to 0,01s were evaluated. In Fig. C.1, a timestep convergence study for case II using the SST model is depicted.

Figure C.1 – Timestep convergence for case II using SST model.

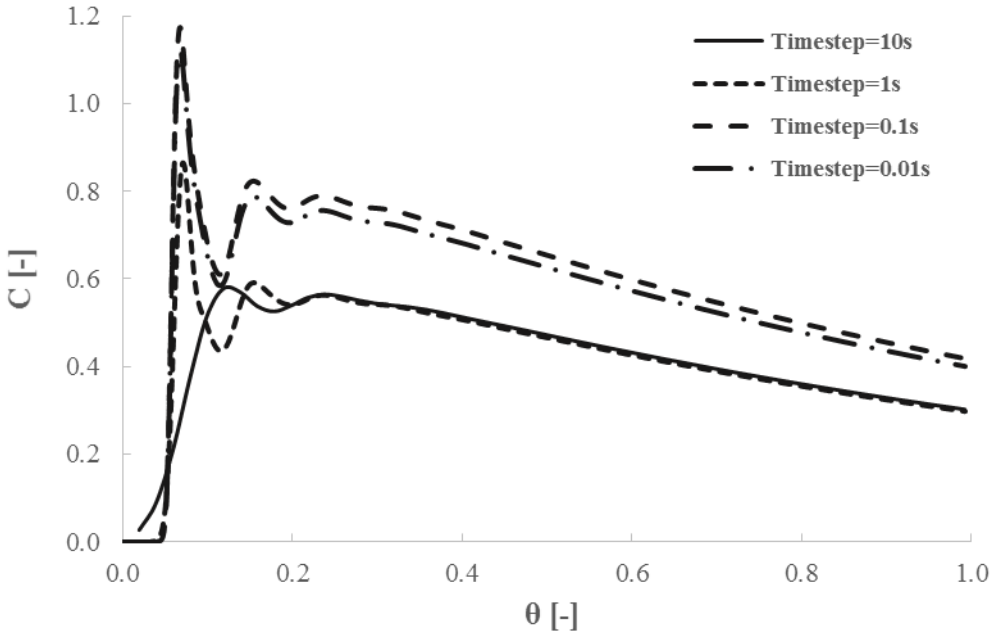

Since the difference between the RTD curves with timesteps of 0,01s and 0,1s were relatively small and aiming to avoid excessive simulation times, we adopted the timestep of 0,1s to represent all case studies presented in this work.

APPENDIX D

INDEPENDENCE TEST FOR PARTICLES INSERTED AT INLET

An independence test to quantify the total amount of particles, which simulates the non-metallic inclusions, inserted at inlet tundish region was performed for all case studies. Particle diameters of $5\,\mu m$, $50\,\mu m$, and $100\,\mu m$ were employed and a number of particles ranging from 20 to 10000 particles was also employed for each particle diameter.

For Lagrangian analysis only the situation with the insertion of the Random Walk Model (RWM) was evaluated. The fraction of removed particles at slag layer for case III, with the RWM is presented in Fig. D.1.

Figure D.1 – Independence test for Case III with the RWM.

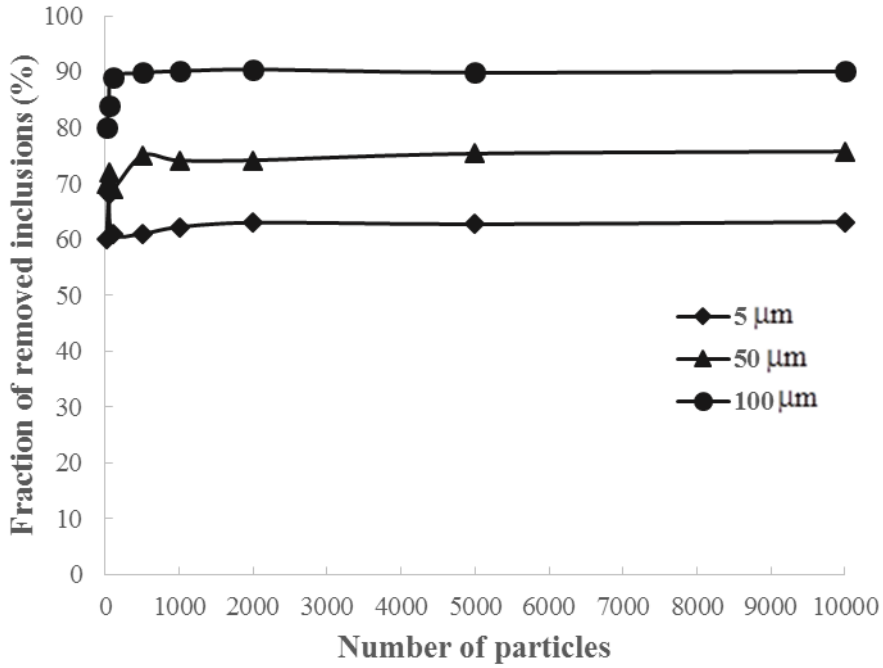

From Fig. D.1 it can be concluded that the difference between the fraction of removed particles at slag layer with 1000 and 10000 particles was minor, therefore, with the goal to avoid excessive simulation times, we chose 1000 particles to represent all case studies presented in this work.